

# **Theoretical Study of Oxygen Ion Conduction Mechanisms in Apatite-type Oxide**

(理論解析を用いたアパタイト型酸化物における酸素イオン伝導機構の解明)

Kouta Imaizumi

今泉 孝太



# Contents

<b>Chapter 1 General Introduction .....</b>	<b>5</b>
1.1 Apatite-type Lanthanum Silicate and Lanthanum Germanate .....	5
1.1.1 Oxygen-ion Conductivity.....	5
1.1.2 Crystal Structure .....	8
1.1.3 Oxygen-ion Conduction Mechanism .....	10
1.2 Outline of This Work .....	11
<b>Chapter 2 Computational Methodology .....</b>	<b>13</b>
2.1 Interstitial Oxygen-ion Sites .....	13
2.2 Oxygen-ion Conduction Pathway and Potential Barrier .....	14
2.3 Oxygen-ion Conductivity .....	17
<b>Chapter 3 Interstitial Oxygen-ion sites .....</b>	<b>19</b>
3.1 Stable Interstitial Sites and Local Structures in $\text{La}_{10}(\text{GeO}_4)_6\text{O}_3$ .....	19
3.2 Stable Interstitial Sites and Local Structures in $\text{La}_{10}(\text{SiO}_4)_6\text{O}_3$ .....	23
<b>Chapter 4 Conduction Mechanism of Interstitial Oxygen Ions .....</b>	<b>26</b>
4.1 $\text{La}_{10}(\text{GeO}_4)_6\text{O}_3$ .....	26
4.1.1 Oxygen-ion Conduction Mechanisms .....	26
4.1.2 Oxygen-ion Diffusivity and Conductivity .....	34
4.1.3 Potential Barrier Height .....	38
4.1.4 Comparison with Previously-proposed Conduction Mechanisms .....	42

4.2	$\text{La}_{10}(\text{SiO}_4)_6\text{O}_3$ .....	46
4.2.1	Oxygen-ion Conduction Mechanisms .....	46
4.2.2	Blocking Effects of Interstitial Oxygen Ion .....	52
4.2.3	Comparison with Previously Reported Mechanisms .....	59
<b>Chapter 5 Effect of Lanthanum-ion Vacancies on Oxygen-ion Conduction .....</b>		<b>62</b>
5.1	Interstitial Oxygen-ion Sites .....	62
5.2	Oxygen-ion conduction mechanisms in $\text{La}_{9.33}(\text{SiO}_4)_6\text{O}_2$ .....	68
5.3	Comparison with Reported Theoretical Mechanisms .....	74
<b>Chapter 6 General Conclusion .....</b>		<b>76</b>
<b>References .....</b>		<b>79</b>
<b>Acknowledgements .....</b>		<b>82</b>

# Chapter 1

## General Introduction

### 1.1 Apatite-type Lanthanum Silicate and Lanthanum Germanate

#### 1.1.1 Oxygen-ion Conductivity

The high oxygen-ion conductivity in oxides having the apatite-type crystal structure was first reported by Nakayama *et al.* in 1995 [1], which inspired motivation of a lot of researchers in the field of solid state ionics to investigate apatite-type oxygen-ion conductors,  $\text{RE}_{9.33+0.67x}(\text{XO}_4)_6\text{O}_{2+x}$  (RE = La, Nd, Sm or Gd ; X = P, Si or Ge). Figure 1.2 shows the reported conductivity curves including other promising oxygen-ion conductors. As seen in the figure, the apatite-type silicate and germanate show higher conductivity than the well-known oxygen-ion conductor, YSZ, especially at intermediate temperatures. In addition, the reported apparent activation energies corresponding to the slopes of the conductivity curves are in the range of 0.6-0.7 eV, lower than those of the YSZ (~ 1.0 eV). This is a great advantage for demand of lowering the operating temperature of SOFCs.

Among the apatite-type oxygen-ion conductors, lanthanum germanate and lanthanum silicate,  $\text{La}_{9.33+0.67x}(\text{MO}_4)_6\text{O}_{2+x}$  (M = Ge or Si,  $0 \leq x \leq 1$ ), have been mainly investigated both experimentally and theoretically due to the highest conductivities in this class at intermediate temperatures [1-3]. As shown in the Fig. 1.1.1, the conductivities of lanthanum silicate

systems show almost linear behaviors with the activation energy of 0.6-0.7 eV. On the other hand, in lanthanum germanate systems, abrupt change in slope of the conductivity curve (from 0.65 eV to 2.07 eV) is observed around 700 °C in  $\text{La}_{10}(\text{GeO}_4)_6\text{O}_3$ , while the similar activation energy is shown at high temperatures ( $>700$  °C). This slope change is reported to be caused by the symmetry change from hexagonal to triclinic during the second-order phase transition, and the high-temperature phase with gentle slope is stabilized by cation doping, as seen in the conductivity curve of the doped lanthanum germanate,  $\text{La}_{9.75}\text{Sr}_{0.25}(\text{GeO}_4)_6\text{O}_{2.5}$ .

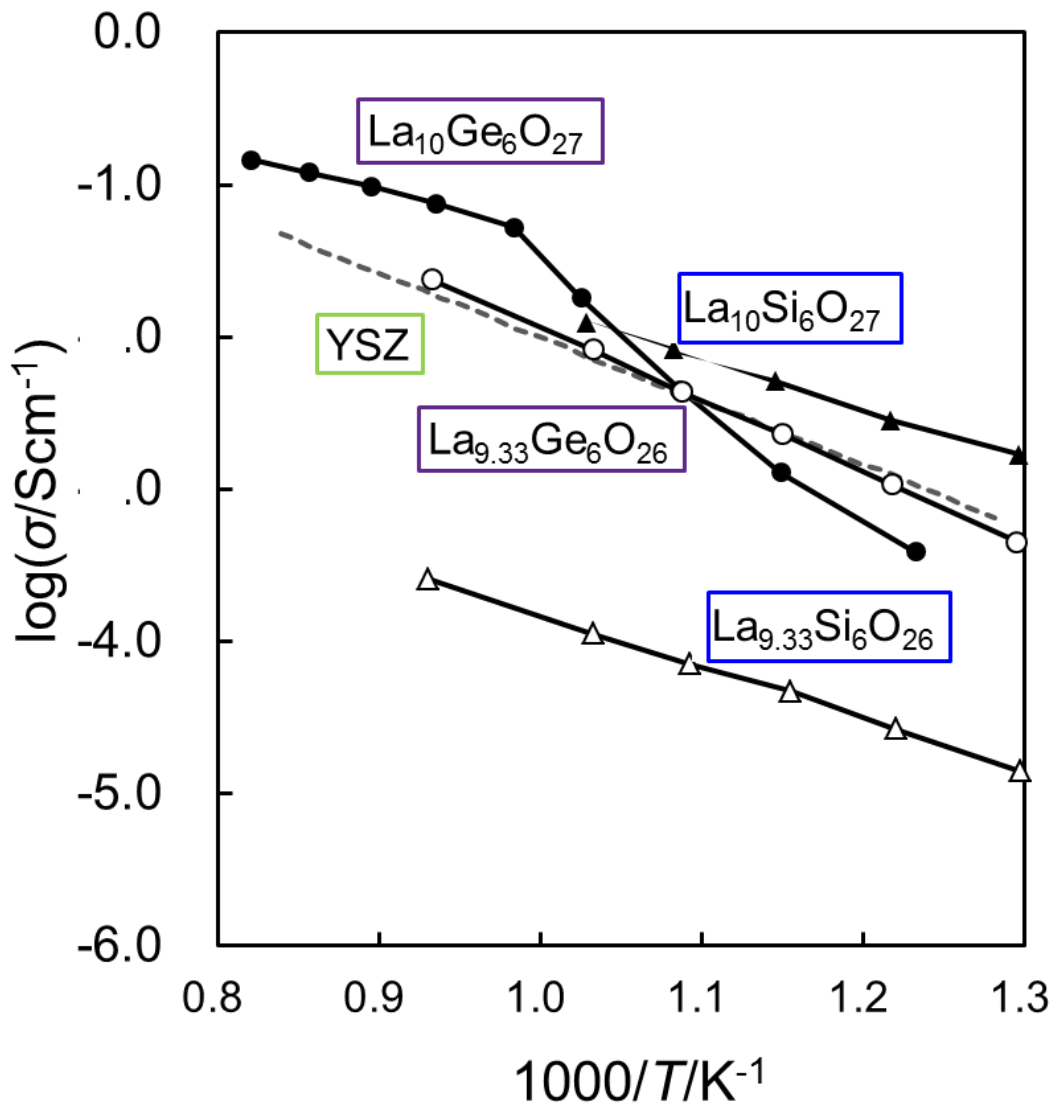
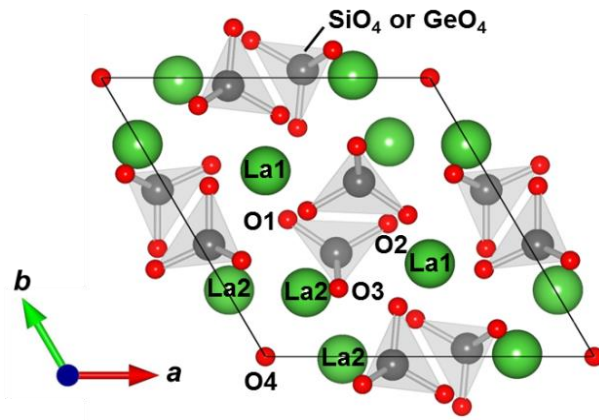


**Figure 1.1.1** The reported oxygen-ion conductivities of lanthanum silicate and germanate systems. The conductivity of another well-known oxygen-ion conductor, YSZ is also shown for reference [3].

### 1.1.2 Crystal Structure

Lanthanum silicate and germanate,  $\text{La}_{9.33+0.67x}(\text{MO}_4)_6\text{O}_{2+x}$  ( $\text{M} = \text{Si}$  or  $\text{Ge}$ ,  $0 \leq x \leq 1$ ) have common hexagonal apatite-type crystal structures with the space group  $\text{P6}_3/m$  as the basic crystal structure. Figure 1.1.3 denotes the crystal structure of lanthanum silicate and germanate. In the crystal structure, crystallographically equivalent two La sites of La1 and La2, one M site, and four O sites of O1~O4 exist. The La2 sites are fully occupied, while the La1 site has 17 % vacancies ( $V_{\text{La}}$ ) at the  $x = 0$  to satisfy the charge neutrality condition. Three of oxygen ions (O1-O3) form the  $\text{MO}_4$  tetrahedra with M ions, and the O4 columns are formed by the remaining O4 ions aligned on the  $c$  axis at even intervals. When the  $x$  composition increases, interstitial oxygen ions are gradually introduced in the crystal, and the La ion fill in the La vacancies to keep the charge neutrality. At the composition of  $x = 1$ , an  $\text{O}_{\text{int}}$  ion are contained per unit cell and the La1 sites are perfectly filled up. The composition changes of  $x > 0$  are reported to drastically enhance the oxygen-ion conductivity [4], which means the interstitial oxygen ions have the important role for the fast oxygen-ion conduction in both systems.

(a) Top view



(b) Side view

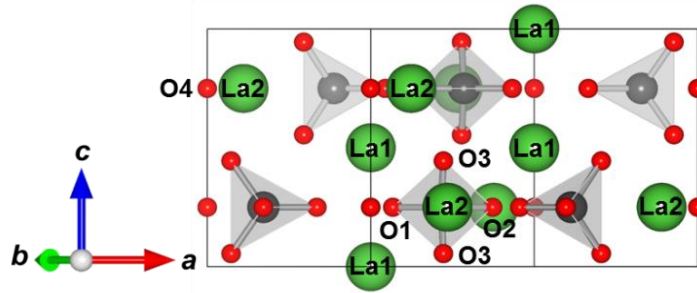


**Figure 1.1.2 Crystal structure of lanthanum silicate and germanate.**

### 1.1.3 Oxygen-ion Conduction Mechanism

As  $O_{\text{int}}$  ions are significantly related to the oxygen-ion conduction in the lanthanum silicate and germanate showed in the above subsection, a number of experimental and theoretical works have been performed to clarify the stable  $O_{\text{int}}$  sites and their conduction mechanisms. In the lanthanum silicate, the stable  $O_{\text{int}}$  site is reported to be located at the periphery of the O4 column in the neutron powder diffraction measurement [5,6], which is also supported by several theoretical analyses using empirical interatomic potentials and first-principles calculations

[7-10]. From these reported  $O_{\text{int}}$  positions in the O4 column, the  $O_{\text{int}}$  ions are considered to migrate over a long range in the O4 column along the  $c$  axis as the dominant fast-conduction pathway. This conduction mechanism is reported to be a cooperative process with O4 ions, so-called “push-pull mechanism” in Fig.1.1.3(a), although the calculated potential barrier of  $\sim 0.3$  eV is lower than reported experimental values [9]. On the other hand, the different cooperative migration mechanisms between  $\text{SiO}_4$  tetrahedra, “hand-over mechanism” in Fig.1.1.3(b), are also reported in lanthanum silicate with increased the composition  $x$ , which is not mentioned the potential barriers.

Similar investigations have also been performed for the lanthanum germanate. The  $O_{\text{int}}$  ion is reported to be stabilized not In the O4 columns but between two neighboring  $\text{GeO}_4$  tetrahedra out of the columns by both experimental and theoretical studies [11-13]. The dominant long-range conduction pathway is proposed between the  $\text{GeO}_4$  tetrahedra along the  $c$  axis by the interstitial mechanism called “fan-like mechanism” with the potential barrier of  $\sim 0.8$  eV in Fig.1.1.3(c) [12]. As another different dominant cooperative conduction mechanism with several oxygen ions, “ $S_{\text{N}}2$ -type processes” in the  $ab$  plane (Fig.1.1.3(d)) is also reported by increasing the composition  $x$ , although the potential barrier is not evaluated quantitatively [13]. Therefore, the holistic dominant conduction mechanism of oxygen ions and the relationships between the compositions and conduction mechanisms are not clarified in the lanthanum silicate and germanate.

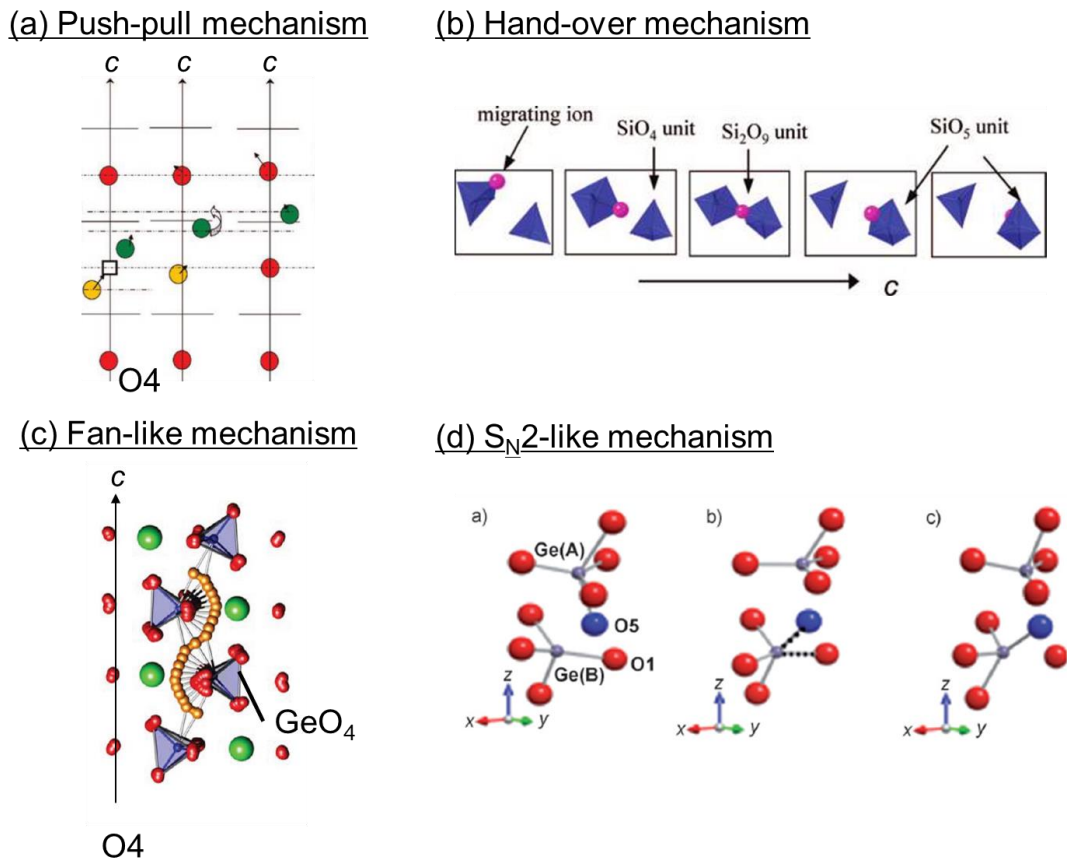


**Figure 1.1.3 Conduction mechanisms in previous works.**

## 1.2 Outline of This Work

From the above brief overview, the oxygen-ion behaviors have not been clarified yet in the lanthanum silicate and germanate systems, though a number of analytical works have been performed so far. In the present study, the oxygen-ion conduction mechanisms in the lanthanum silicate and germanate have been theoretically re-examined on the basis of first-principles calculations, to propose the true picture of oxygen-ion conduction behavior in both systems. The outline of the present thesis is as

follow.

At first, computational methods involving the nudged elastic band (NEB) method and kinetic Monte Carlo (KMC) simulations used in this study and their calculation conditions of each method are showed in chapter 2. Next, energetically stable sites for the interstitial oxygen ion in both lanthanum germanate,  $\text{La}_{10}(\text{GeO}_4)_6\text{O}_3$ , and lanthanum silicate,  $\text{La}_{10}(\text{SiO}_4)_6\text{O}_3$ , are investigated and discussed the difference of the stable sites between both the crystal systems. Based on the obtained results of the stable interstitial sites in  $\text{La}_{10}(\text{GeO}_4)_6\text{O}_3$  and  $\text{La}_{10}(\text{SiO}_4)_6\text{O}_3$  in chapter 2, the oxygen-ion conduction pathways and mechanisms in both crystals are quantitatively evaluated using the NEB methods and KMC simulations from the energetic point of view in chapter 4. In chapter 5, the same investigations in chapter 4 performed for the  $\text{La}_{9.33}(\text{GeO}_4)_6\text{O}_2$  having lanthanum vacancies in order to clarify the effects of the lanthanum compositions for the oxygen-ion conduction mechanisms. Finally, the brief summary of this study is provided in Chapter 6.

## Chapter 2

### Computational Methodology

#### 2.1 Interstitial Oxygen-ion Sites

Before finding the oxygen-ion conduction mechanisms, low-energy interstitial oxygen-ion sites were investigated using the structural relaxation based on the first-principles calculations. In order to roughly estimate the stable sites of interstitial oxygen-ions, initial interstitial sites and crystal structures were determined by the potential energy surface (PES) calculated by static lattice simulations used in the General Utility Lattice Program (GULP) code [14]. As the short-range and long-range interactions between constituent ions, the two-body Buckingham potentials and the Coulomb potentials were used during the calculations, respectively [9]. The shell model is applied for ionic polarization, where an ion is considered to be consisted of the charged shell and shell connected by a harmonic spring [15]. After the determinations for the several local energy minima sites of the interstitial oxygen ion in the constructed PES, structural optimization by first principles calculations was performed for them with the convergence condition of residual forces  $< 0.02 \text{ eV/\AA}$  for all atoms. In this study, projector augmented wave (PAW) method using the VASP code applied for all electronic structure calculations [16-21]. As valence states in the PAW potentials, the  $5s$ ,  $5p$ ,

6s and 5d orbitals for La, 4s and 4p orbitals for Ge, 3s and 3p orbitals for Si, and 2s and 2p orbitals for O were treated. The generalized gradient approximation (GGA) was used as the exchange-correlation terms [22]. The cutoff energy of expanded electronic wave functions by plane waves set to 400 eV. Supercells consisting of 1×1×2 or 1×1×3 unit cells of  $[\text{La}_{9.33+x}(\text{GeO}_4)_6\text{O}_2]^{2+}$  or  $[\text{La}_{9.33+x}(\text{SiO}_4)_6\text{O}_2]^{2+}$  ( $x = 0$  or 0.67) were used as the host lattice with 2×2×1  $k$ -point sampling. The accuracy of each calculation cell used two host lattices are confirmed by comparing the experimental data as shown in Table 2.1.1, which is in good agreement with the error from the experimental data within 1 %.

Table 4.1.1 lattice parameter of lanthanum germanate and silicate. Numerals in parentheses represent the experimental values [11, 36]

格子定数	$\text{La}_{10}(\text{GeO}_4)_6\text{O}_3$	$\text{La}_{10}(\text{SiO}_4)_6\text{O}_3$	$\text{La}_{9.33}(\text{GeO}_4)_6\text{O}_2$
$a (= b)$ (Å)	9.84 (9.93)	9.60 (9.71)	9.90 (9.91)
$c$ (Å)	7.30 (7.30)	7.19 (7.18)	7.25 (7.30)

## 2.2 Oxygen-ion Conduction Pathway and Potential Barrier

After determination of the interstitial sites and stable structures in the crystals, the conduction pathways and mechanisms connecting interstitial sites were investigated using nudged elastic band (NEB) method. The NEB method was used for evaluation of energy profiles for all the possible

conduction paths of interstitial oxygen ions [23]. This method can quantitatively evaluate minimum energy paths (MEP) and their potential energy barriers connecting the initial and final states while the FPMD simulations can qualitatively provide possible conduction processes in the crystals. In the NEB method, mobile ions arrange at equal distances between initial and final states as transition positions and connect each neighboring ion by imaginary springs shown like the figure 2.2.1. Next, the total force  $F_i$  of each ion is calculated by structural optimization according to the following equation:

$$F_i = -\nabla V(R_i) + \{\nabla V(R_i) \cdot q_i\}q_i + \{k[(R_{i-1} - R_i) + (R_{i+1} - R_i)] \cdot q_i\}q_i \quad (2-2-1)$$

where  $V(R_i)$  is potential surface on the position  $R_i$ ,  $q_i$  is unit vector of the tangential direction for the mobile direction at position  $R_i$  and  $k$  is spring constant. The perpendicular force of mobile direction is evaluated by first and second terms, which means the each ion of transition state is restrictedly optimized on the vertical surface of the mobile direction. The third term indicates summation of spring forces connecting the neighboring ions along the tangential direction for the mobile direction, which keep each mobile ion at the equal interval during structural optimization. As the initial and final states of interstitial oxygen-ion conduction, the stable interstitial oxygen-sites determined in chapter 3 were used. The each atomic position of transition states were optimized with the convergence condition of  $F_i < 0.05 \text{ eV/\AA}$ .

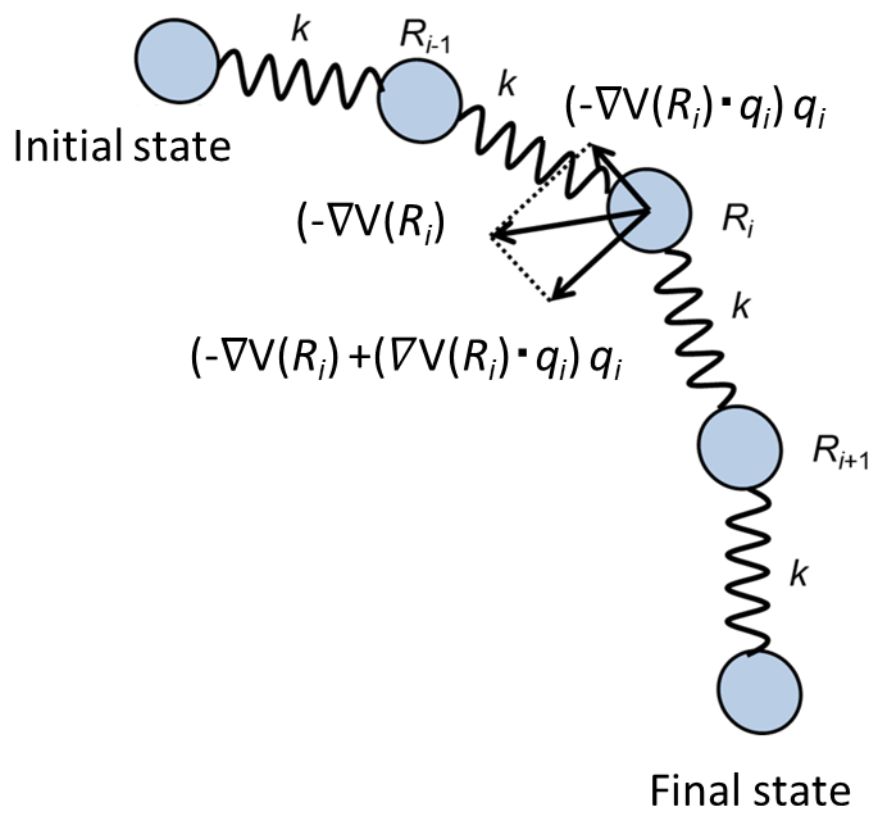


**Figure 2.2.1 Restrain condition of calculation ions in the NEB method.**

## 2.3 Oxygen-ion Conductivity

The KMC simulations were conducted in order to estimate the oxygen-ion conductivities in the crystals [24,25]. In this simulation, the mobile ions and their interstitial sites set in the crystals based on the results of the chapter 3 and 4 at first. Next, the jump events to the next neighboring site were performed for mobile ions, which was stochastically determined from the mean jump frequency ( $\nu$ ) calculated from the potential barrier ( $\Delta E$ ) of each conduction pathway by the following relations:

$$\nu = \nu^* \exp(-\Delta E/k_B T), \quad (2-3-1)$$

where the Boltzmann constant is represented by  $k_B$ ,  $T$  is the temperature, and the vibrational prefactor is denoted by  $\nu^*$  that was set to be  $10^{13}$  THz. After repetition of these jump events, the oxygen-ion diffusivities were calculated by the definitional following equation:

$$D_{x_i} = \lim_{n \rightarrow \infty} \langle r_{x_i,n}^2 / 2t_n \rangle, \quad (2-3-2)$$

Where a direction in the crystal is denoted by  $x_i$ , and the shift vector and times after  $n$ -times jump repetitions of  $x_i$ -component are represented by  $r_{x_i,n}$  and  $t_n$ , respectively. After the carefully checking the convergence of the evaluated diffusivities, the KMC simulation steps,  $n$ , were determined to  $1 \times 10^5$  steps. The averaged diffusion coefficients are calculated after 10,000 times repetitions per a trial in the range of temperature from 500 to 1500 K. The oxygen-ion conductivities were finally given from the calculated diffusivities by the following equations,

$$B_{x_i} = 2eD_{x_i}/k_B T, \quad (2-3-3)$$

$$\sigma_{x_i} = 2eC_{O_{int}} B_{x_i}, \quad (2-3-4)$$

where  $B$ ,  $2e$ ,  $\sigma$  and  $C$  is the mobility, the charge of interstitial oxygen ions, the oxygen-ion conductivity, and the concentration of interstitial oxygen ions, respectively.

## Chapter 3

### Interstitial Oxygen-ion sites

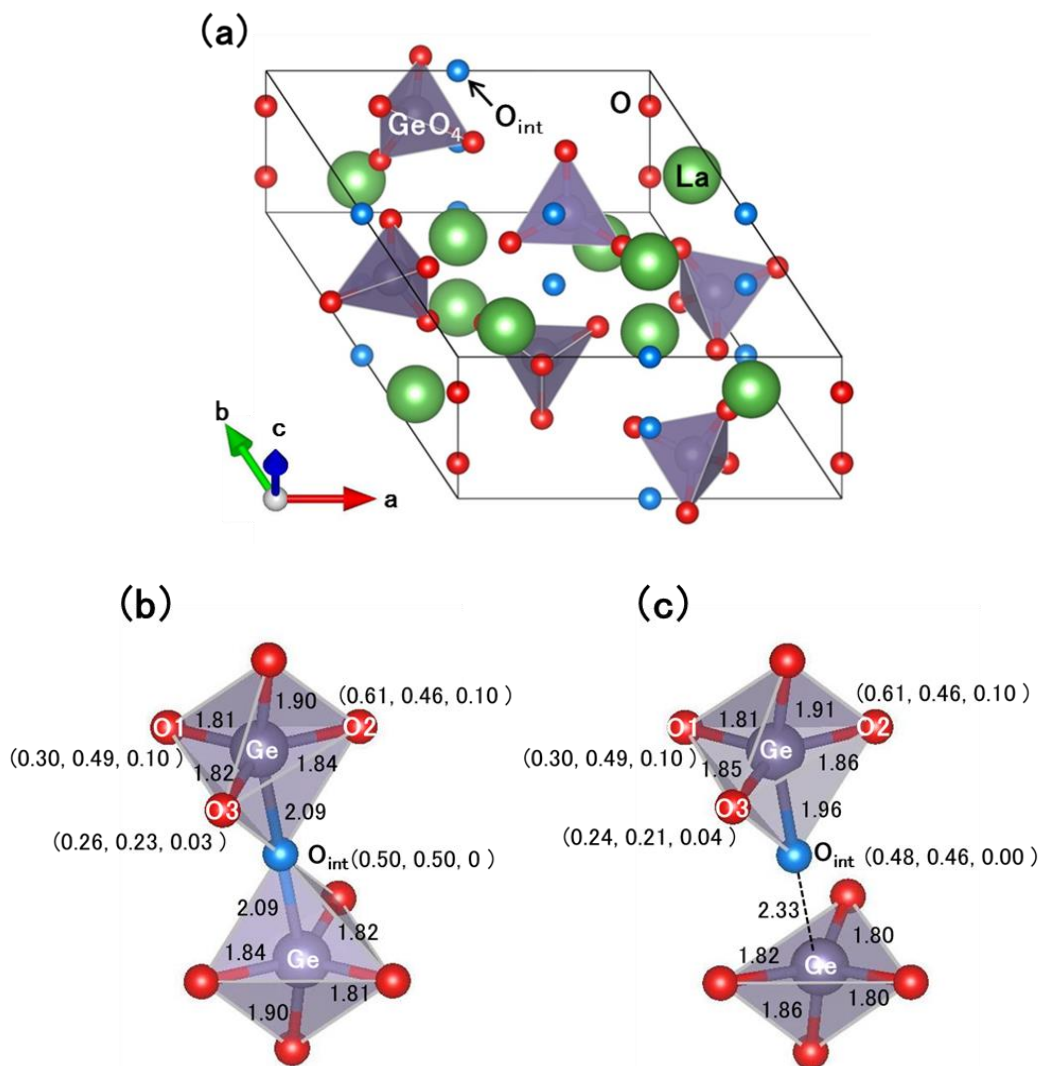
#### 3.1 Stable Interstitial Sites and Local Structures in $\text{La}_{10}(\text{GeO}_4)_6\text{O}_3$

Figure 3.1.1a shows the most stable sites of interstitial oxygen ions described on the unit cell structure, which were determined by the first-principles calculations. All the crystallographically equivalent interstitial oxygen-ion sites are superimposed in the figure according to the  $P6_3/m$  symmetry. The interstitial oxygen ions are located at the highly symmetric position (0.5, 0.5, 0) in the fractional coordinate, existing six equivalent sites per unit cell. As the structurally optimized local structure of Fig. 3.1.1b, the interstitial oxygen ion forms a  $\text{Ge}_2\text{O}_9$  unit with two neighboring  $\text{GeO}_4$  tetrahedra where the interstitial oxygen ion is located at the center between the two  $\text{GeO}_4$ . The distances between two Ge ions and the interstitial oxygen ion in the  $\text{Ge}_2\text{O}_9$  unit are both 2.09 Å and the other eight Ge-O distances are in the range from 1.8 Å to 1.9 Å, which are longer than those of  $\text{GeO}_4$  tetrahedra in the structure of  $\text{La}_{10}(\text{GeO}_4)_6\text{O}_2$  without an interstitial oxygen ion (1.7 Å to 1.8 Å). Similar local  $\text{Ge}_2\text{O}_9$  unit was also reported in static lattice simulations of  $\text{La}_{9.33}(\text{GeO}_4)_6\text{O}_2$  by Kendrick *et al* [12].

Interstitial oxygen-ion sites between neighboring  $\text{GeO}_4$  tetrahedra

were theoretically and experimentally reported by Orera *et al.* and Pramana *et al.*, respectively [11,26]. They performed the static lattice calculations based on empirical inter-atomic potentials and the neutron powder diffraction measurements. However, the local structures around interstitial oxygen ions were expressed as  $\text{GeO}_5$  hexahedra instead of  $\text{Ge}_2\text{O}_9$  units in these papers, because the interstitial oxygen ion was deviated from the center between the two  $\text{GeO}_4$  toward one  $\text{GeO}_4$  unit. Pramana *et al.* reported that the deviation of interstitial oxygen ion site from the center is  $0.45 \text{ \AA}$ , which seems not to be coincide with the most stable interstitial oxygen-ion sites in this study. However, it was also found from our investigations that the interstitial oxygen-ion site is not unique at that site and those having similar total energies (less than  $0.08 \text{ eV}$  difference ) are located within a radius of  $\sim 0.3 \text{ \AA}$  from the center stable site  $(0.5, 0.5, 0)$ . Moreover, the averaged position of the interstitial oxygen ion observed in the FPMD simulations for 90 ps at 1000 K was almost  $(0.5, 0.5, 0)$  and the spatial distribution of the interstitial oxygen ion during the FPMD calculations were also almost centered at the averaged position. These results indicate the energetically favorable zone to interstitial oxygen ions widely ranges around  $(0.5, 0.5, 0)$  between two  $\text{GeO}_4$  units. Therefore, the deviation of the interstitial sites in the previous experiments may result from locally low symmetry by impurities and/or point defects. In fact, the interstitial oxygen-ion site was reported to be deviated from the center position in  $\text{La}_{8+x}\text{Ba}_{2-x}(\text{GeO}_4)_6\text{O}_{2+0.5x}$  and  $\text{La}_8\text{Y}_2(\text{GeO}_4)_6\text{O}_3$  containing Ba and Y dopants by some computational studies [13,26]. The differences

in the interstitial oxygen-ion site between our computational studies and their experimental can be recognized as the reasonable.



**Figure 3.1.1 (a) All the interstitial oxygen-ion sites in  $\text{La}_{10}(\text{GeO}_4)_6\text{O}_3$ . The local structure around an interstitial oxygen ion at (b)  $(0.5, 0.5, 0)$  with  $\text{Ge}_2\text{O}_9$  unit and (c) the asymmetric interstitial site found by calculations by using  $1 \times 1 \times 3$  unit cells. The red and blue balls mean the regular and interstitial sites of oxygen-ions, respectively. Numerals represent bond lengths ( $\text{\AA}$ ) and the numbers in parentheses denote the atomic coordinates of oxygen-ions.**

### 3.2 Stable Interstitial Sites and Local Structures in $\text{La}_{10}(\text{SiO}_4)_6\text{O}_3$

Figure 3.2.1a shows the most stable and metastable sites of interstitial oxygen ions. The crystallographically equivalent interstitial oxygen-ion sites are shown in the figure by the same colors, according to the  $P6_3/m$  symmetry. The interstitial oxygen ions in  $\text{La}_{10}(\text{SiO}_4)_6\text{O}_3$  are located at two areas, i.e., the most stable zones and the metastable zones. In the most stable zone, equivalent six sites ( $\text{O}_{\text{int-1}}$  site: blue balls) with the representative position (0.04, 0.04, 0.01) in the fractional coordinate are closely located at the periphery of the O4 columns. In the metastable zone, on the other hand, two metastable interstitial sites ( $\text{O}_{\text{int-2}}$  site: dark gray balls,  $\text{O}_{\text{int-3}}$  site: light gray balls) are located between two  $\text{SiO}_4$  tetrahedra, whose positions and site energies are (0.46, 0.43, 0.00) with 0.29 eV and (0.50, 0.47, -0.02) with 0.49 eV against that of the most stable site, respectively. The each positions of the metastable sites are deviated from the center position (0.5, 0.5, 0) of two  $\text{SiO}_4$  tetrahedra to a  $\text{SiO}_4$  tetrahedron, forming a  $\text{SiO}_5$  hexahedra as shown in Fig. 3.2.2b. These two stable zones for interstitial oxygen ions in the lanthanum silicate are reasonably consistent with the previously-reported interstitial oxygen-ion sites in both experimental and theoretical studies, although the reported fractional coordinates are deviated slightly from those in this study because of the effects of dopants and/or La vacancies [5,10,27].

In this study, the interstitial sites in  $\text{La}_{10}(\text{GeO}_4)_6\text{O}_3$  and  $\text{La}_{10}(\text{SiO}_4)_6\text{O}_3$  indicate the large differences although the apatite-type crystal structures

are the same between two crystal. The interstitial oxygen ions in  $\text{La}_{10}(\text{GeO}_4)_6\text{O}_3$  are the most stabilized between neighboring two  $\text{GeO}_4$  tetrahedra with the local structures of  $\text{Ge}_2\text{O}_9$  units. As evaluation of the stability around  $\text{GeO}_4$  tetrahedra, the structural optimization was performed for the crystal structure with the interstitial oxygen ion located at the O4 column which is the most stable interstitial site in  $\text{La}_{10}(\text{SiO}_4)_6\text{O}_3$ , however, the interstitial site did not exist by relaxing the interstitial ions toward the  $\text{GeO}_4$  tetrahedra. On the other hand, the interstitial sites in  $\text{La}_{10}(\text{SiO}_4)_6\text{O}_3$  are located at both the surround of the O4 column and interspace of two  $\text{SiO}_4$  tetrahedra as the most stable and meta-stable sites, respectively. These differences of the interstitial sites between the  $\text{La}_{10}(\text{GeO}_4)_6\text{O}_3$  and  $\text{La}_{10}(\text{SiO}_4)_6\text{O}_3$  are considered to result from the gap between the bonding strengths of Ge-O and Si-O for the interstitial oxygen ion. While Ge ions around the interstitial oxygen ion in  $\text{La}_{10}(\text{GeO}_4)_6\text{O}_3$  are comparatively coordinated to multi-O ions like the local structure of  $\text{Ge}_2\text{O}_9$  unit, Si ions are less coordinated with O ions than that of Ge ion in  $\text{La}_{10}(\text{SiO}_4)_6\text{O}_3$ , which results in that stability of the interstitial site in the O4 column without Si-O bondings exceeds that of the local structures of  $\text{SiO}_5$  hexahedra or  $\text{Si}_2\text{O}_9$  units. In fact, comparing the most stable phases between  $\text{GeO}_2$  and  $\text{SiO}_2$  oxides,  $\text{SiO}_2$  is stabilized as the quartz structure with fourfold coordinated Si ions although the most stable phase of  $\text{GeO}_2$  is the rutile structure having sixfold coordinated Ge ions.

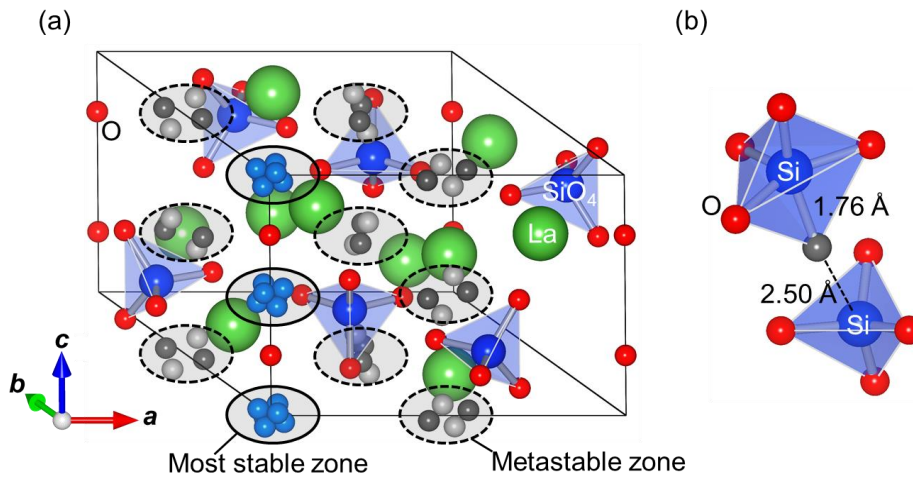


**Figure 3.2.1 (a) Most stable and metastable sites of the interstitial oxygen ions in the lanthanum silicate. The blue ball indicates the most stable site of O<sub>int-1</sub> site, and the two metastable sites of O<sub>int-2</sub> and O<sub>int-3</sub> sites are denoted by the dark and light gray balls, respectively. The most stable and metastable zones are described by the Solid and dotted circles. The local structure around an O<sub>int-2</sub> ion is shown in (b).**

## Chapter 4

### Conduction Mechanism of Interstitial Oxygen Ions

#### 4.1 $\text{La}_{10}(\text{GeO}_4)_6\text{O}_3$

##### 4.1.1 Oxygen-ion Conduction Mechanisms

From the obtained interstitial stable sites, migration pathways between neighboring interstitial sites were subsequently calculated with their energy profiles using the NEB method. In the present study, simple interstitial conduction mechanism and cooperative migration mechanisms by several oxygen ions were considered. The migration paths by the interstitial and cooperative interstitialcy mechanisms along the  $c$  axis with their energy profiles show in Fig. 4.1.1. Figure 4.1.1a show the interstitial mechanism, where the interstitial ion moves at the circumference of a  $\text{GeO}_4$  tetrahedron to go directly into the adjacent interstitial site having a large 1.27 eV of the potential barrier shown in Fig. 4.1.1c. Fig. 4.1.1b show, on the other hand, the cooperative migration involving the two oxygen ions at the regular and interstitial sites was considered. In this conduction, the interstitial ion goes along the  $c$  axis and pushes the other oxygen ion at the regular site into the adjacent interstitial site (Fig. 4.1.2). Then, it was found that the evaluated potential barrier is 0.64 eV (solid line in Fig. 4.1.1c), almost a half in that by the interstitial mechanism. Therefore, the dominant long-range conduction pathway of interstitial ions

along the  $c$  axis is given by the repetition of this cooperative mechanism.

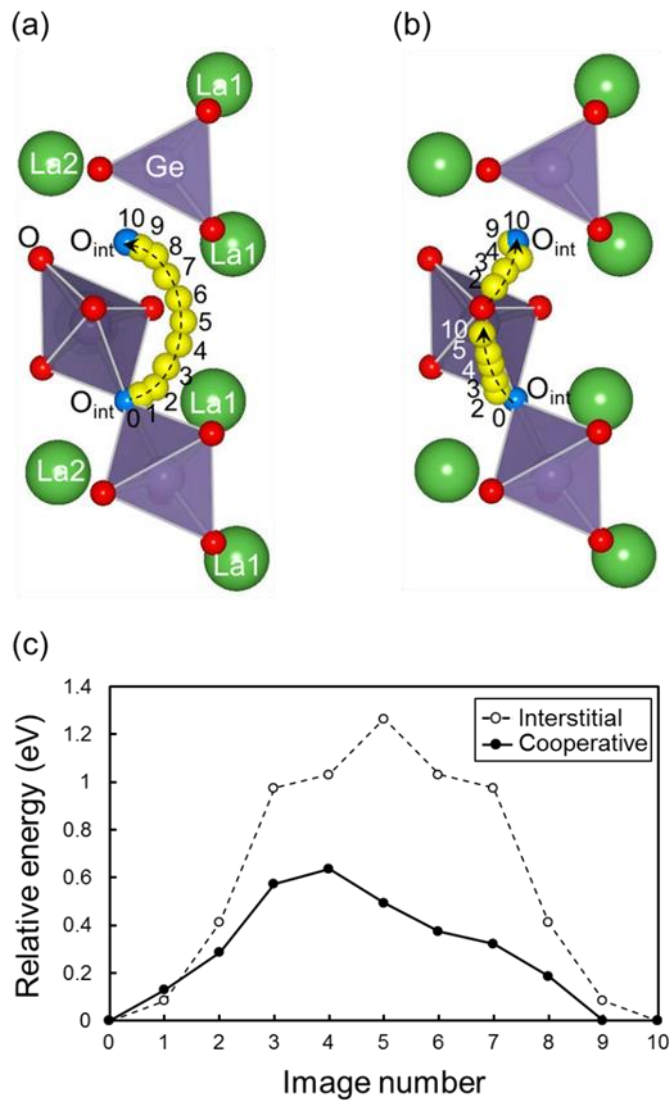


**Figure 4.1.1** The migration trajectories of oxygen ion along the  $c$  axis by (a) the simple interstitial and (b) the cooperative mechanisms. The yellow and blue spheres mean the trajectories of the migration paths and interstitial sites, respectively. (c) The energy profiles during the migrations. The interstitial and the cooperative mechanism are described as broken line and solid line, respectively. The numbers of the yellow spheres denote the image numbers.

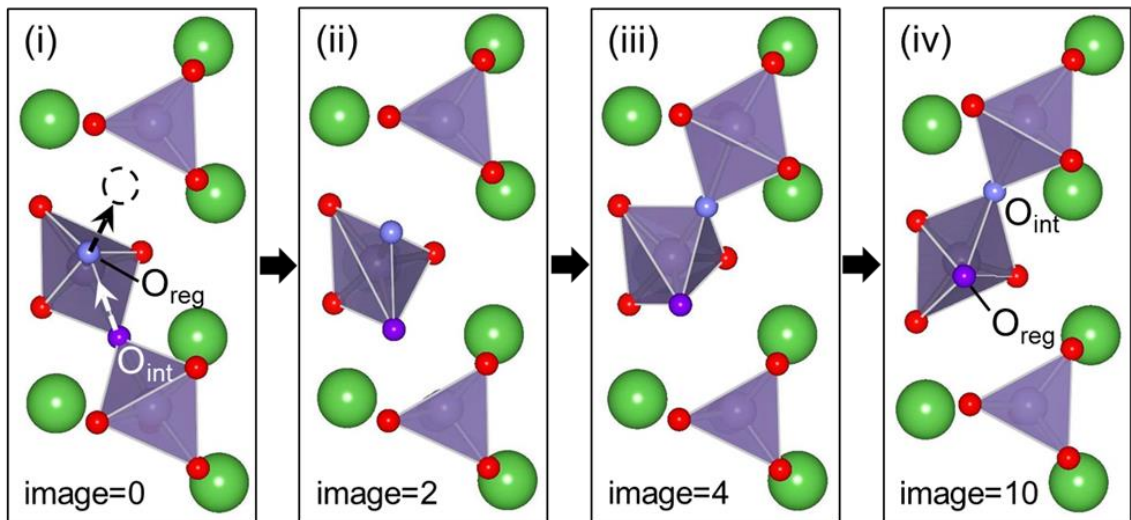


**Figure 4.1.2** The migration processes along the  $c$  axis by the interstitialcy mechanism. The image = 0, 2, 4, 10 in Fig. 3c are described (i) ~ (iv), respectively. The mainly mobile oxygen ions are represented by light and dark purple spheres.  $O_{\text{reg}}$  and  $O_{\text{int}}$  denote the oxygen ions at regular and interstitial sites, respectively. Moving directions during the conduction are shown by the arrows.

Secondly, oxygen-ion migration in the *ab* plane was investigated. The migration paths in the *ab* plane connecting the migration pathways along the *c* axis are shown in Fig. 4.1.3. Figure 4.1.3a show the migration process by the interstitial conduction mechanism connecting the adjacent interstitial sites in the *ab* plane. The conducting interstitial ion is located far from any  $\text{GeO}_4$  tetrahedra breaking the Ge-O bond during the transition state in this process, when the calculated energy relatively becomes the highest (2.55 eV in Fig. 4.1.3c). In the cooperative conduction process including three oxygen ions at two regular sites and one interstitial site as shown in Fig. 4.1.3b, on the other hand, the interstitial ion pushes firstly an oxygen ion at a regular site in the same  $\text{Ge}_2\text{O}_9$  unit toward the adjacent  $\text{GeO}_4$  tetrahedron. The oxygen ion pushed out from the  $\text{Ge}_2\text{O}_9$  unit tends to occupy the regular oxygen-ion site of the adjacent  $\text{GeO}_4$  tetrahedron, and the former regular oxygen ion of the  $\text{GeO}_4$  tetrahedron instead migrates to the nearest interstitial site. Though this cooperative conduction process by three oxygen ions is not simple, the potential barrier decreases to 1.17 eV for the inter-channel oxygen-ion migrations in the *ab* plane. However, the potential barrier in the *ab* plane is still higher than that along the *c* axis.

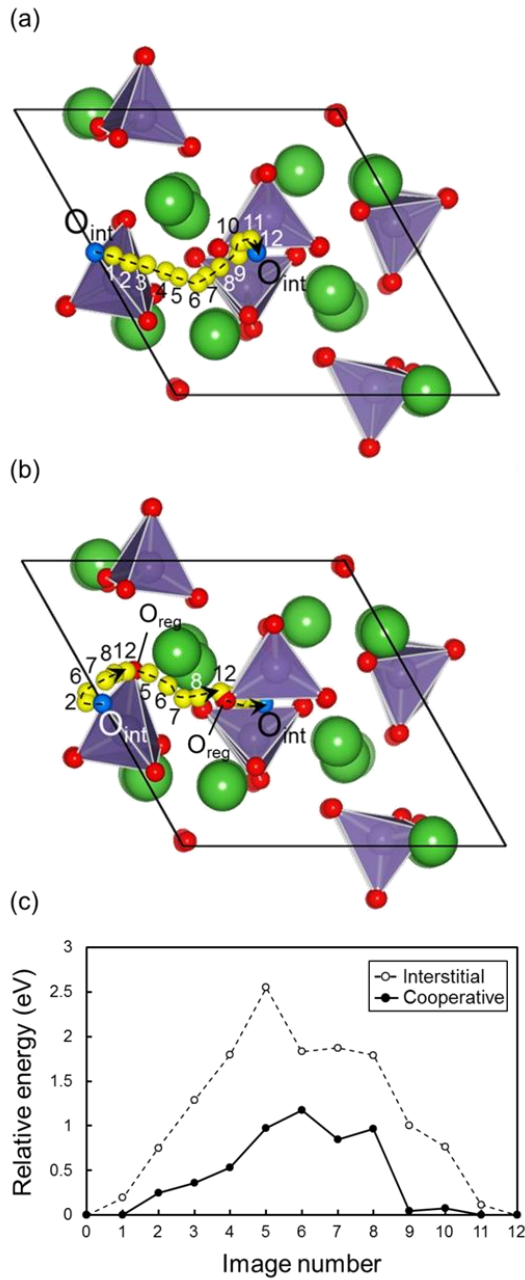


**Figure 4.1.3 (a)(b) The conduction pathways of oxygen-ion conduction processes between the adjacent interstitial sites in the  $ab$  plane by (a) the interstitial and (b) the interstitialcy mechanisms. The evaluated energy profiles in the two migration processes are shown in (c).**

$\text{La}_{10}(\text{GeO}_4)_6\text{O}_3$  seems to have the significant anisotropic migrations of oxygen ion along the  $c$  axis according to the above results. In our previous FPMD calculations, however, additional migration pathways in the  $ab$  plane was also observed, shown in Fig. 4.1.4 and 4.1.5. In this conduction path, four oxygen ions at one interstitial, two regular sites in  $\text{GeO}_4$  tetrahedra, and one O4 ion are cooperatively migrated, which can be mentioned as “multi- oxygen ion cooperative mechanism”. During the migration process, the O4 ion neighboring to the interstitial ion gets out from the O4 column to form a  $\text{GeO}_5$  unit as the first step (Fig. 4.1.5(ii)), and Fig. 4.1.5(iii) shows an oxygen ion in a  $\text{GeO}_4$  tetrahedron at the regular site subsequently moves into the vacant site at the O4 column. Then, the  $\text{GeO}_5$  unit are simultaneously formed to a  $\text{Ge}_2\text{O}_9$  unit with a adjacent  $\text{GeO}_4$  unit and the oxygen ion at original interstitial site occupies the regular site in  $\text{GeO}_4$  tetrahedra (Fig. 4.1.5(iv)), finally to complete the conduction processes of interstitial oxygen ion. During this complicated migration, a metastable state exists when two  $\text{GeO}_5$  units are temporarily formed as shown in Fig. 4.1.5(ii). The potential barrier of this conduction pathway is evaluated 0.76 eV, which is much lower potential barrier than the interstitial and cooperative mechanisms as shown in Fig. 4.1.3. Therefore, “multi- oxygen ion cooperative mechanism” via O4 columns are the dominant pathways in the  $ab$  plane.

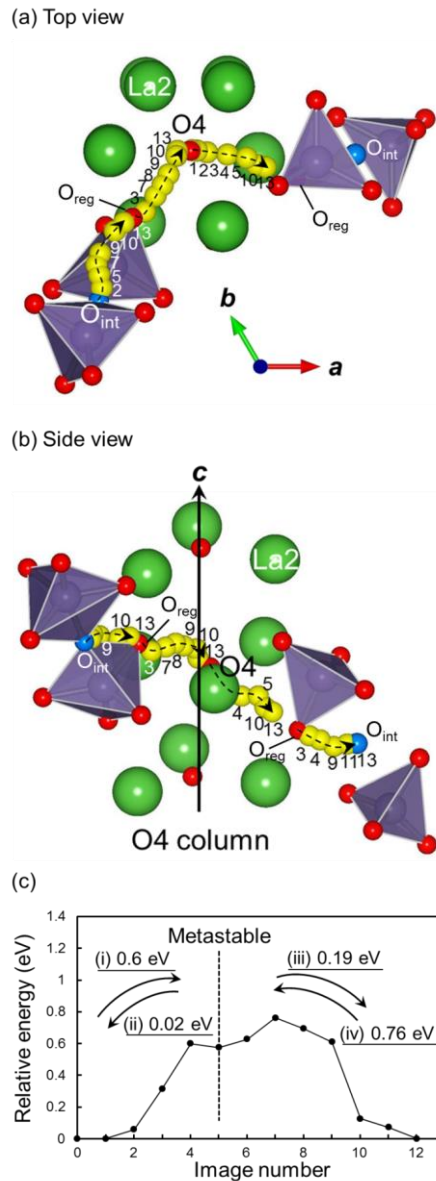


**Figure 4.1.4 (a)(b) The conduction pathways of the migration process via the O4 column. The yellow and blue spheres mean the trajectories of oxygen ions and the interstitial sites, respectively. The calculated energy profile is shown in (c). Four elementary processes during the migrations of (i) ~ (iv) are shown in the figure(c).**

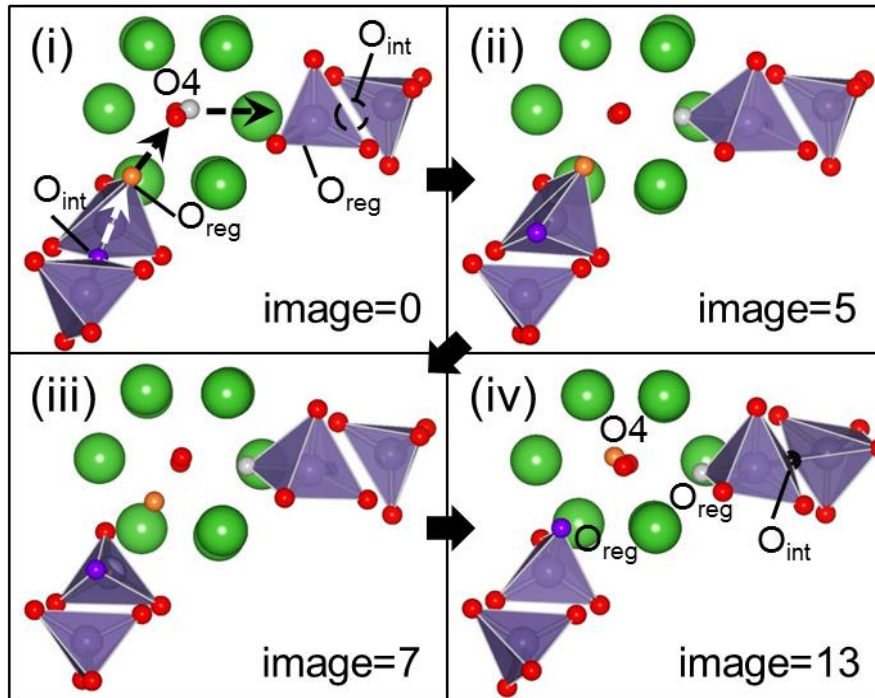


**Figure 4.1.5** The detailed migration process via the O4 column. The mainly mobile oxygen ions are denoted by black, gray, orange, and purple spheres during the migrations. The snapshots of (ii) is the metastable state (image 5) and (iii) indicates the highest potential energy state (image 7).  $O_{\text{reg}}$  and  $O_{\text{int}}$  denote the oxygen ions at regular and interstitial sites, respectively. Moving directions during the conduction are shown by the arrows.

#### 4.1.2. Oxygen-ion Diffusivity and Conductivity

Diffusion simulations of the mobile interstitial oxygen ions were performed on the basis of the KMC method to evaluate the oxygen-ion conductivity in  $\text{La}_{10}(\text{GeO}_4)_6\text{O}_3$ . In this simulation, the cooperative migration mechanisms having the low potential barriers below 1 eV were taken into account. The oxygen-ion conductivities along the  $c$  axis and in the  $ab$  plane are shown in Fig. 4.1.6. The apparent activation energies corresponding to the gradients of slope in the conductivity curve along the  $c$  axis and in the  $ab$  plane are 0.67 eV and 0.75 eV, respectively, which are almost correspond to the potential barriers of the long-range conduction along the  $c$  axis and via the O4 column by the cooperative mechanisms, respectively. The averaged conductivity which means the conductivity in realistic polycrystals randomly-oriented, is also indicated by broken line in the figure with the apparent activation energy of 0.71 eV.

Although the almost isotropic conductivity are found by “the multi-oxygen ion cooperative mechanism” in the  $ab$  plane, the conduction pathways along the  $c$  axis remain dominant slightly in the range of this temperature, particularly at the low temperature zone. The event rates of the migration steps along the  $c$  axis and via the O4 column at the temperatures of 500, 1000 and 1500 K show in Table 4.1.1. In the migration process via the O4 column with a metastable state, four elementary steps exist (See Fig. 4.1.4c), i.e., (i) from the initial state to the metastable state, (ii) from the metastable state back to the initial state, (iii)

from the metastable state to the final state (equivalent to the initial), and (iv) the final state to the metastable state. In the figure, the evaluated potential barrier heights of each step which are referenced to the potential barrier of initial states are additionally indicated. From the figure and table, it is found that the difference in the mean frequencies of each step evaluated from the potential heights result in the discrepancy between event rates of the migration processes. Event rates of the steps (i) and (ii) are quite high compared to the other steps, however these two steps are the repeating states only between the initial and metastable states, which means the high rates of steps (i) and (ii) are not contributing to migrations for long range diffusions. Therefore, steps (iii) and (iv) are rate-controlling processes in “the multi-oxygen ion cooperative mechanism” via the O4 column, whose event rates should be compared with that of conduction along the  $c$  axis. Comparing the event rates at 500 K, those of steps (iii) and (iv) is lower than that along the  $c$  axis by one-order of magnitude, which suggests the conduction along the  $c$  axis is dominant. The discrepancy of mean frequencies between conduction along the  $c$  axis and via the O4 column decreases with increasing the temperature, which results in almost equal event rates and isotropic oxygen-ion conductivity around 1500 K.

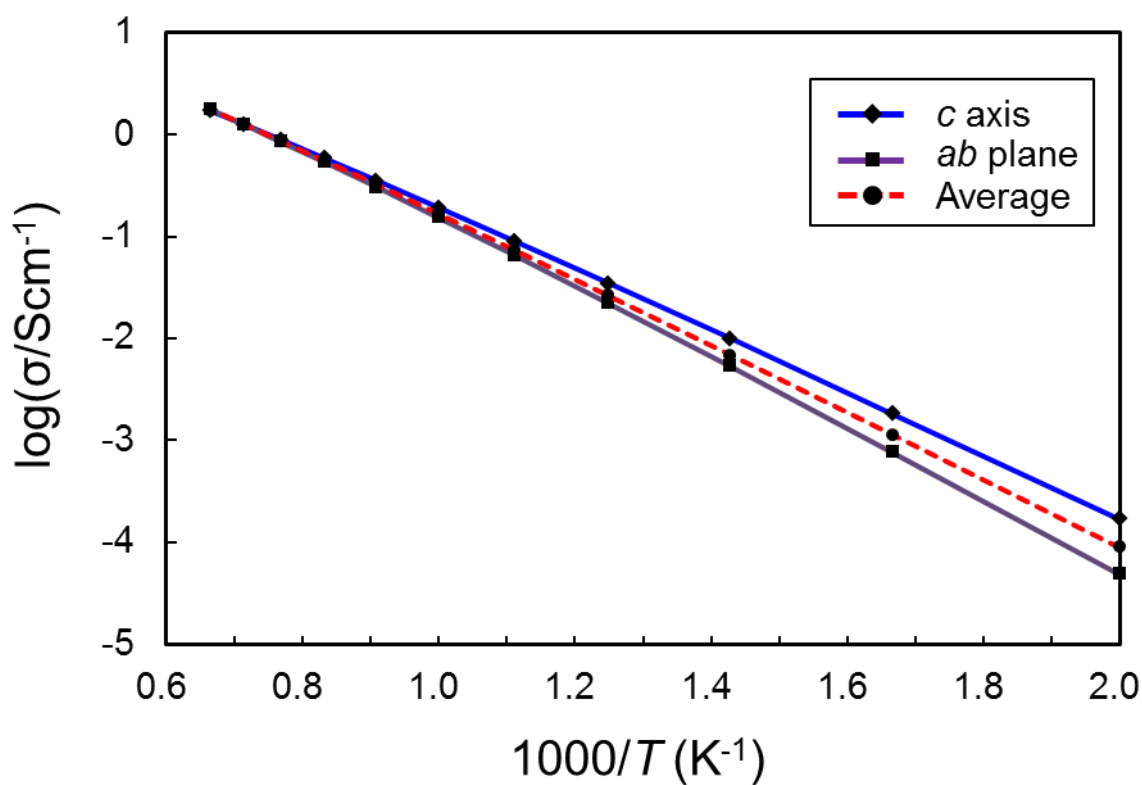


**Figure 4.1.6** The calculated oxygen-ion conductivities along the *c* axis (blue line), in the *ab* plane (purple line) plotted against the inverse temperature estimated by the KMC simulations. The averaged conductivity is denoted by red broken line.

**Table 4.1.1** Frequencies of the migration events both along the  $c$  axis and via the O4 column at the temperature of 500, 1000, and 1500 K. The four elementary processes in the migration in Fig. 4.1.4c correspond to (i) ~ (iv) in the table.

Temperature	Along $c$ axis	Via O4 column			
		(i)	(ii)	(iii)	(iv)
500 K	16.9 %	40.6 %	40.7 %	1.0 %	0.8 %
1000 K	20.4 %	34.4 %	34.9 %	5.4 %	4.9 %
1500 K	20.6 %	30.8 %	31.2 %	8.9 %	8.5 %

### 4.1.3. Potential Barrier Height

The evaluated potential barriers show large differences according to migration processes, e.g., “along the *c* axis vs. in the *ab* plane” and “interstitial vs. cooperative mechanisms”. The reasons of the difference are discussed qualitatively by focusing the chemical bonding and local structure changing. Especially, Ge-O bonds and the interaction of the electrostatic repulsion between neighboring oxygen ions are focused on.

The effects of Ge-O bonds for potential barriers during the oxygen ion migrations can be recognized notably by comparing the interstitial conduction processes between along the *c* axis and in the *ab* plane. In figures 4.1.7a and 4.1.7b, the energy profiles with Ge-O<sub>int</sub> distance change during the conduction processes along the *c* axis and in the *ab* plane is shown. In the interstitial conduction mechanism along the *c* axis, the Ge-O<sub>int</sub> length is slightly decrease from 2.06 Å (image 0) to 1.90 Å (image 5) by forming a GeO<sub>5</sub> unit, which shows the Ge-O<sub>int</sub> bond is not almost changed during the migration. On the other hand, the Ge-O<sub>int</sub> distance during the conduction in the *ab* plane by interstitial mechanism is reached 2.46 Å at a maximum, which means the Ge-O<sub>int</sub> bond is broken. Therefore, the high potential barrier of 2.55 eV is considered to be caused by the interaction of no Ge-O<sub>int</sub> bonding.

As the other important factor to decide the potential barrier, the interaction of electrostatic repulsion between oxygen ions is clarified by comparing the potential barriers and local structures during the migrations

in between the cooperative interstitialcy and the interstitial mechanisms. The O-O lengths of the first- (1NN) and second- (2NN) nearest neighbor at each migration state in the cooperative and interstitial mechanisms are shown in figures 4.1.8a and 4.1.8b. In the interstitial mechanism, the mobile interstitial oxygen ion is gradually close to adjacent oxygen ions. At the middle state of image 5, both O-O lengths of 1NN and 2NN become the shortest with the highest potential energy. Relationship between energy profile and O-O length show similar tendency in the cooperative mechanism, which means the intermediate state of image 4 indicates the shortest O-O length with the highest potential energy. However, potential barrier of the cooperative mechanism is low compared to that of the interstitial mechanism because the O-O lengths of 1NN and 2NN are kept totally constant in the cooperative migration. By contrast, the O-O lengths of the 1NN and 2NN become short in the interstitial process. This is why the cooperative processes enable to show lower potential barriers by less effect of O-O repulsions compared to the interstitial process.

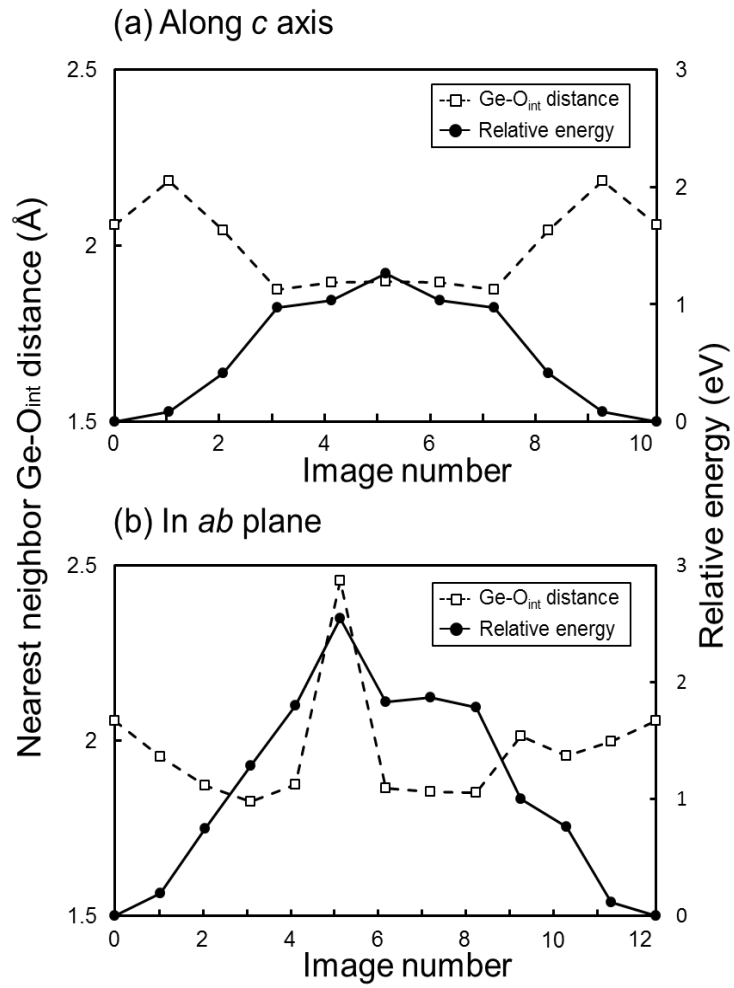


**Figure 4.1.7** The relative energy (solid line) and the nearest Ge-O<sub>int</sub> length (broken line) in each state of the oxygen ion conductions (a) along the *c* axis and (b) in the *ab* plane by the interstitial mechanisms.

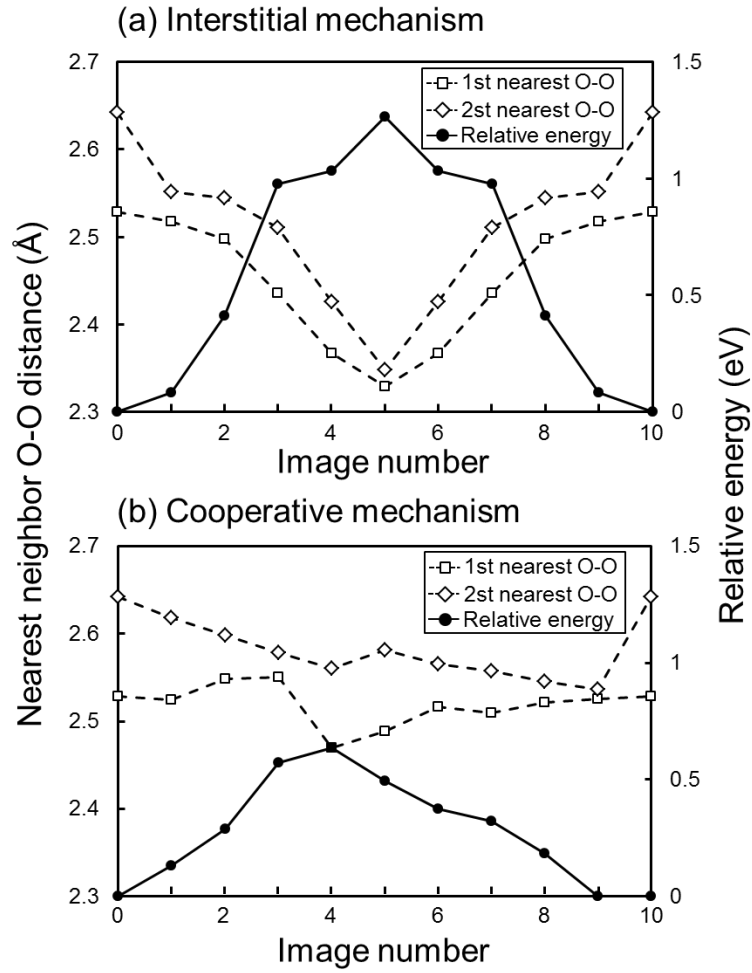


**Figure 4.1.8** The relative energy denoted by solid line and the lengths of the first- and second-nearest O-O ions denoted by broken line in each state of the oxygen ion conduction by (a) the interstitial and (b) the cooperative mechanisms along the *c* axis.

#### 4.1.4. Comparison with Previously-proposed Conduction Mechanisms

A number of oxygen-ion migration mechanisms have theoretically been reported before in the lanthanum germanate systems. For example, the interstitial mechanism along the  $c$  axis, so-called “fan-like mechanism” with apparent activation energy of 0.79 eV was proposed in the MD simulation by Kendrick *et al.* [12]. The potential barrier of 1.27 eV in the same interstitial mechanism (Fig. 4.1.1a), however, indicates higher in the present study, which results from the discrepancy in computational technique, i.e., first-principles calculations vs. MD simulations on the basis of the experimental ionic potentials. Instead, the cooperative interstitialcy mechanism along the  $c$  axis is found as the long-range conduction pathway having the lowest potential barrier of 0.64 eV in this study, which corresponds to the dominant migration pathway in this system. Panchmatia *et al.* also previously reported the cooperative conduction mechanism in the  $ab$  plane, “S<sub>N</sub>2-type process” as the dominant conduction mechanism from MD calculations using empirical interatomic potentials [13]. Although the authors did not mention the potential barrier for the mechanism, the calculated potential barrier of the similar cooperative mechanism in the present study (Fig. 4.1.3b) was, however, 1.17 eV, which is much higher than the potential barrier of the conduction along the  $c$  axis (0.64 eV). Furthermore, the dominant conduction mechanism in the  $ab$  plane is the multi-oxygen ion cooperative

mechanism via the O4 column with lower potential barrier of 0.76 eV (Fig. 4.1.4), rather than such the  $S_N2$ -type process.

Here, the differences of conduction mechanisms between  $La_{10}(GeO_4)_6O_3$  and lanthanum silicate ( $La_{9.33+0.67x}(SiO_4)_6O_{2+x}$ ) are discussed. In lanthanum silicate, the most stable interstitial site is located at around the O4 column, which reported by both theoretical and experimental study [5,10,27]. Additionally, the most stable site between two tetrahedra in  $La_{10}(GeO_4)_6O_3$  found in the present study is proposed as a metastable site in lanthanum silicate by Matsunaga *et al* [10]. The discrepancy in the local minima sites leads to migration behavior-change of oxygen ions between germanate and silicate systems. In silicate, some interstitial and interstitialcy mechanisms along the *c* axis in the O4 column, so-called “sinusoidal-like pathway” and “push-pull type mechanism” were reported as the dominant migration paths, which are quite different from the dominant migration paths through the interspaces between  $GeO_4$  tetrahedra in the germanate. “ $S_N2$ -type process” was also reported as the inter-channel migrations pathways connecting the fast pathways along the O4 column in the silicate [28], although the similar migration process is not contributed to the dominant conduction in the germanate. Thus, the two apatite-type oxygen-ion conductors have quite difference for migration pathways and mechanisms by the discrepancy of stable sites between lanthanum germanate and silicate in spite of the same crystal structure.

The oxygen-ion conductivity of  $La_{10}(GeO_4)_6O_3$  was experimentally

reported [3,29,30], whose Arrhenius plots show the large change in slope around 1000 K. This slope change is considered to be the second-order phase transition from the hexagonal phase at high-temperature to the triclinic phase at low-temperature. The apparent activation energy is reported as 0.65 eV and 1.80 eV at high temperatures over 1000 K and at temperatures from 750 K to 1000 K, respectively. The oxygen-ion conductivity calculated in this study means to the high-temperature phase because the hexagonal crystal structure was used in the present calculations. The averaged apparent activation energy obtained by the diffusion calculations is 0.71 eV, which is in good agreement with the experimentally reported activation energy. In addition to the activation energies, conductivity of  $5.5 \times 10^{-1}$  S/cm estimated as quantitative values in this simulation is also reasonable much to the experimental conductivities,  $1.4 \times 10^{-1}$  S/cm, in the same order of magnitude at 1200 K [3].

The investigations for the influences of La vacancies and/or some types of dopants at La site on the activation energy of oxygen-ion conductivity curve were also performed experimentally in previous study. The oxygen ion conductivities at two compositions of the lanthanum germanate ( $x = 0, 0.34$  in  $\text{La}_{9.33+x}(\text{GeO}_4)_6\text{O}_{2+x}$ ) which is different concentrations of La vacancies were measured by Abram *et al.* [29]. In comparison between the compositions of  $x = 0$  and 0.34, both apparent activation energies are around 0.8 eV with almost the same conductivities in the high-temperature area. These apparent activation energies are slightly high compared with

0.71 eV in the present result, which is considered to be result from the discrepancy of local structures around La sites. On the other hand, enhancement of the oxygen ion conductivity in the range of low temperatures was reported by doping several cations on the La site. The effect of cation doping is decrease to the temperature of the phase transition. Therefore, the gradual slope of conductivity in the hexagonal high-temperature phase with the low activation energy expands to the low-temperature area [3]. From the conductivity measurements for  $\text{La}_9\text{M}(\text{GeO}_4)_6\text{O}_{2.5}$  (M= Ca, Sr, Ba) by Pramana *et al.*, the apparent activation energies of each compositions are 0.70, 0.71, and 1.01 eV, respectively, in the range of high-temperature phase [30], which indicates that doping Ca and Sr ions are ideal to improve the oxygen-ion conductivity in lanthanum germanate system because they can expand the low activation energy region keeping the low value of 0.71 eV in the ideal system of  $\text{La}_{10}(\text{GeO}_4)_6\text{O}_3$ .

## 4.2 $\text{La}_{10}(\text{SiO}_4)_6\text{O}_3$

### 4.2.1 Oxygen-ion Conduction Mechanisms

Possible elementary processes of interstitial oxygen-ion conduction between interstitial sites obtained in chapter 3.2 were calculated by the NEB calculations. The elementary processes can be grouped into two types. One is “short-range paths within 1 Å in the stable zones” and the other is “middle-range paths with 3–4 Å distances connecting the adjacent stable zones”. The group of short-range paths can be classified additional two subtypes. Subtype (I) is “the most stable zone” and subtype (II) is “the metastable zone”. The group of middle-range paths can be also classified into three types, (III) “between most stable zones”, (IV) “between a most stable and a metastable zones”, and (V) “between metastable zones”.

At first, the migration paths in the group of short-range paths were investigated. In the subtype (I), the potential barriers of short migration paths between the equivalent six  $\text{O}_{\text{int}-1}$  sites are all below 0.01 eV, which indicates the interstitial ion can migrate frequently between close the most stable sites. In the subtype (II), on the other hand, the potential barriers of the short migration paths between the four sites (equivalent two sites of each  $\text{O}_{\text{int}-2}$  and  $\text{O}_{\text{int}-3}$ ) show relatively high, 0.32 eV at minimum.

Next, the calculations for the group of the middle-range migration paths connecting the each stable zone were performed, which are

necessary to determine the long-range migration pathways of oxygen ions. The migration pathway of the lowest potential barrier in subtype (III) which is elementary process between most stable zones in the O4 column along the  $c$  axis is shown in figure 4.2.1(a). During the conduction process, an interstitial ion and O4 ion located at the intermediate site move cooperatively to the next adjacent  $O_{\text{int}}-1$  site along the  $c$  axis, whose migration mechanism is the same conductive type of the “push-pull mechanism” reported in previous studies [11, 13]. The calculated potential barrier is, however, extremely low (less than 0.01 eV), which does not coincide with the conventional potential barriers in ionic conduction (~ few tenths eV). In the previous theoretical investigation of  $\text{La}_{9.33}(\text{SiO}_4)_6\text{O}_2$  involving La vacancies [13], the potential energy height of the same migration paths by the push-pull mechanism was calculated, which is 0.3 eV higher than that in this study of composition of no La vacancies. The main reason of the relatively-high potential barrier in  $\text{La}_{9.33}(\text{SiO}_4)_6\text{O}_2$  is the split of interstitial sites at the periphery of the O4 column into four sites by decreasing the crystallographic symmetry attributed to the introduction of La vacancies, whose site energies are ranged from 0 to 0.25 eV. Thus, the push-pull migration mechanism in the O4 column essentially exists as the very fast-conduction pathways in the ideal composition without defects including La vacancies. This fast ion migration with low potential barrier is probably resulted from the short moving distances of migration ions due to the cooperative

interstitialcy conduction process involving O4 ions. In fact, O4 and interstitial ions moved only 0.66 Å from the initial to final positions during migrations, which is almost the same to migration lengths in the short-range paths in the most stable zone (subtype(I)).

In the subtype (IV) which is the elementary migration processes connecting the most stable and the metastable zones, the lowest potential barrier are found by the cooperative migration process by two mobile oxygen ions at an regular O3 and a  $O_{\text{int-1}}$  sites as shown in figure 4.2.1(b). During the process, the interstitial oxygen ion gradually gets out from the  $O_{\text{int-1}}$  stable site in the O4 column to the O3 site in a adjacent  $\text{SiO}_4$  tetrahedron. At the same time of interstitial-ion motion, the O3 ion in the  $\text{SiO}_4$  tetrahedron moves to the  $O_{\text{int-2}}$  metastable site. The calculated potential barrier of this elementary step is 0.58 eV with reference to site energy of the most stable site.

The elementary process and its energy profile in subtype (V) which is the migration pathway connecting two  $O_{\text{int-2}}$  sites between  $\text{SiO}_4$  tetrahedra along the  $c$  axis are shown in figure 4.2.1(c). During the migration process, the reorientation of  $\text{SiO}_5$  hexahedral unit was considered to be conducted by not rotation but deformation of the hexahedron. Oxygen ions at a metastable site cooperatively migrate with O2 ions at regular sites along the  $c$  axis, whose potential barrier is evaluated 0.53 eV with reference to the site energy of  $O_{\text{int-2}}$  site, in other words, 0.82 eV with reference to that of the most stable site.

The long-range pathways of oxygen-ion migration can be formed by repeating and combining the obtained elementary processes. The long-range conduction pathways along the  $c$  axis in the O4 column are shown by the light purple balls in figure 4.2.2(a), which is formed by repeating only the cooperative mechanism (push-pull mechanism) in the O4 column mentioned in subtype(III). The potential barrier of this long-range pathways along the  $c$  axis is extremely-low, which causes the strong anisotropy during the oxygen-ion conduction as measured conductivities in previous studies using highly-oriented pellets and single crystals [31, 32]. It shows similar trend between theoretical and experimental results, however, it is not reasonable in principle that only the migration pathway in one-dimensional narrow zone such as O4 column realizes as the long-range conduction, because mobile interstitial ions conducting along the one-dimensional columns are expected to definitely not migrate to long-range by frequently blocking by their neighbor ions during the migrations.

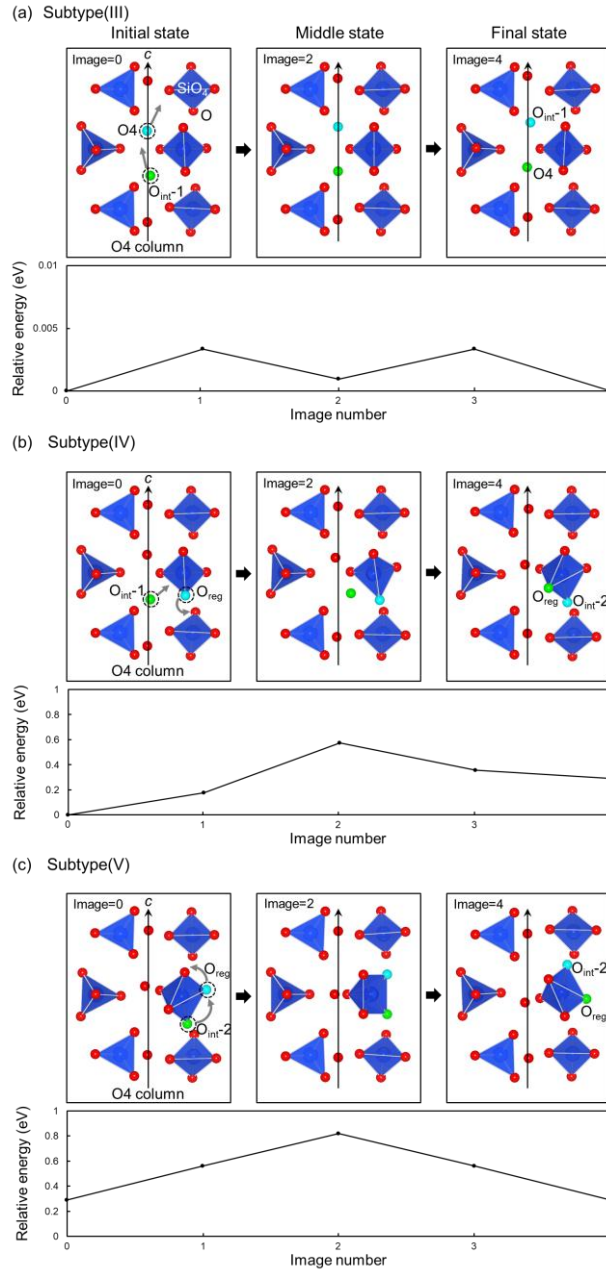


**Figure 4.2.1** The snap shots during the elementary conduction processes and their energy profiles (a) between the most stable  $O_{int-1}$  sites in the O4 column long the  $c$  axis, (b) between the  $O_{int-1}$  sites and the metastable  $O_{int-2}$  sites in the  $ab$  plane, and (c) the  $O_{int-2}$  sites along the  $c$  axis. The the regular sites of oxygen ions represent as  $O_{reg}$ . The the blue and light green balls and the arrows means two conducting oxygen ions and their motion directions, respectively.

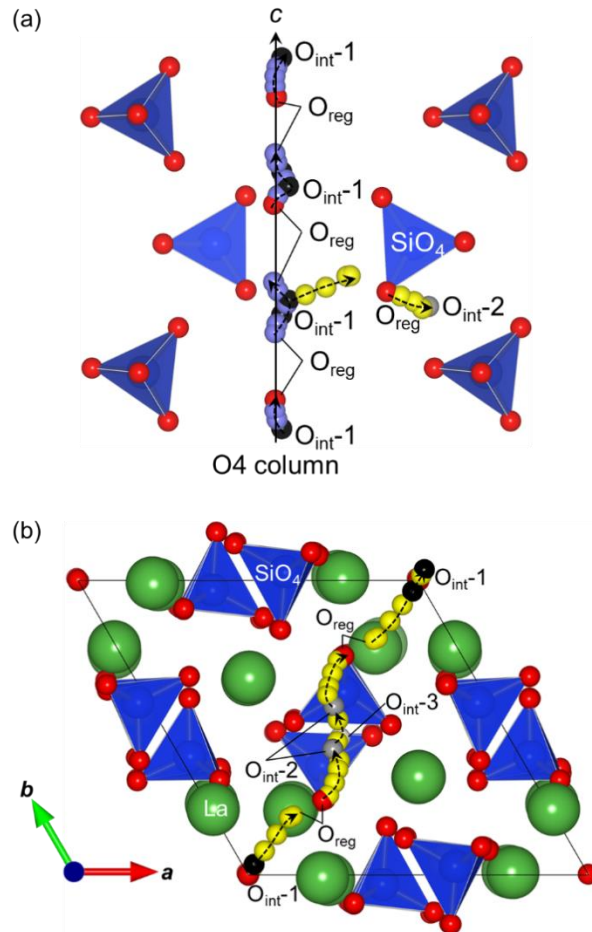


**Figure 4.2.2.** (a) The long-range pathway of oxygen-ion migration along the  $c$  axis in the O4 column (light purple balls) and the getting-out mechanism from column (yellow balls). (b) The long-range pathway of oxygen-ion migration in the  $ab$  plane. The  $O_{int-1}$ ,  $O_{int-2}$  and  $O_{int-3}$  sites are represented by black, gray, and white balls, respectively. The  $O_{int}$  and  $O_{reg}$  mean the interstitial and regular sites, respectively.

### 4.2.2 Blocking Effects of Interstitial Oxygen Ion

In order to confirm the blocking effect between interstitial oxygen ions in the O4 column during the migrations, the stochastic simulations for the correlated behaviors of the interactive interstitial oxygen ions were performed by the KMC method. As the migration pathways, all obtained elementary processes were used except the short-range pathways in the most stable zone to be simplified the diffusion simulations. The six equivalent sites in most stable zone regards as a single site during the simulations by the following two reasonable presumptions. One is the very-fast interstitial conduction in the single zone is negligible because of not effect to the total diffusivity. The other is the mobile ions are not permitted to be located simultaneously at over two sites in the same zone because this situation is too close each mobile ion to be definitely occurred in realistic conductions. In the calculations, different-sized supercells of  $1 \times 1 \times N$  unit cells which is stacking along the  $c$  axis by  $N = 3, 9, 27, 81$  and  $243$  were used with the periodic boundary condition. The number of interstitial ions in the cell corresponds with the supercell size  $N$  because the interstitial ion concentrations in unit cell is kept one in all the supercells. Here, it is important precondition that even the length along the  $c$  axis direction of the largest supercell ( $N = 243$ ) is only 175 nm, which is much smaller than conventional thickness

of the electrolytes to apply as the fuel cells and samples to measure the ion conductivity. Therefore, the interstitial oxygen-ion dynamics in realistic crystals must be discussed by extrapolating the situation at  $N = \infty$  condition from the evaluated data in the diffusion simulations.

The diffusion coefficients of interstitial oxygen ions along the  $c$  axis calculated by the displacements from initial into final positions in each different-sized supercells shows in figure 4.2.3(a) as a function of inverse temperature. From the graph, the larger the supercell size  $N$  is, the steeper the slope of the diffusivity curve becomes, which means the interstitial ions lose the mobility in the larger collective scale. In figure 4.2.3 (b), the correlation factors of interstitial-ion diffusion along the  $c$  axis ( $f_{//c}$ ) shows against the inverse  $N$  ( $N^{-1}$ ) at 500, 1000, and 1500 K. The correlation factors is set as the ratio to the diffusivity of a independent interstitial ion ( $f_{//c} = D_{//c}/D_{//c}^{\text{independ}}$ ), which means the interaction effect between interstitial ions on the diffusion coefficients. They are proportional to  $N^{-1}$  through the origin at 500 K, while deviation from the linearity appears at elevated temperatures.

The linear relation between  $N^{-1}$  and the correlation factors at 500 K is resulted from the long-range collective motions by interstitial ions in the O4 column over the periodic boundary of the finite-sized supercells. The frequency of the push-pull mechanism during the

simulation at this low temperature is over 99.999 % corresponding to the extremely low potential barrier shown in Fig.4.2.3 (c), so that the conduction of interstitial ion is almost confined within the single O4 column. Therefore, each interstitial ion in the one-dimensional O4 column cannot overtake the two adjacent mobile ions, which means the initial relationships of sequential arrangement between mobile ions is kept during the diffusions. This limitation by the interactions of adjacent mobile ions is the blocking effect, which makes the mobile interstitial ion diffuse only by the collective movement with all the interstitial ions in the O4 column. Here, the ion diffusion in the finite-sized supercells enables long-range collective movement by considering the periodic boundary along the column, where the interstitial ions can come back into the supercell from the opposite side by crossing the boundary. Such collective movements of interstitial ions in the simulation affect more critically for smaller supercells, where the rate of the interstitial ions movement in unison is relatively higher in spite of their random motions in principles. The linear dependence of the correlation factor as a function of  $N^{-1}$  is very important because it means no collective movement in the large- $N$  limit, equal to negligible diffusivity of the interstitial ions. Therefore, the diffusivities of the interstitial ions in realistic crystal are much small compared with the estimated one from the push-pull mechanism with the extremely-low potential height due to the strong interruption of long-range migrations by the blocking effect.

The correlation factors depart from the proportional relation and converge the constant value in the large- $N$  limit at the high temperature of 1500 K because the frequency of getting-out mechanism to the push-pull mechanism increase from  $\sim 0.6\%$  at 1000 K to  $\sim 4\%$  at 1500 K as shown in in figure 4.2.3 (d). The getting-out mechanism drawn as yellow ball in figure 4.2.2(a)) can make the interstitial ions refuge temporarily from the densely packed O4 column to a metastable site as guidepaths. Interstitial ions arranged in the O4 column can overtake their neighbors by this mechanism, enabling their large displacements without the collective movement. The blocking effect is, therefore, relaxed gradually with elevating temperatures contributed by the increase of the event rate of the getting-out mechanism. The constant values at the large- $N$  limit which is deviated from the linearity mean the true diffusivities in realistic systems. The apparent activation energy of the diffusion coefficient curve at the large- $N$  limit corresponds to the potential barrier of the getting-out mechanism (0.58 eV) in principle, whose tendency can be found in by comparing the diffusivity curve at  $N = 243$  and the inserted triangle in figure 4.2.3(a).

Thus, it is found that the strong interactions between mobile ions by the blocking effect must be considered such the diffusions of interstitial ion densely packed along the one-dimensional O4 column. The getting-out mechanism enable this blocking effect to relax, which is the dominant diffusion mechanism. In principle, the

blocking effect certainly occurs in all correlated diffusions within a narrow one-dimensional pathway, in which the by-paths such as the getting-out mechanism in the lanthanum silicate is necessary and the rate-determining process for the long-range migration pathway. However, the diffusion simulations using finite-sized cells with the periodic boundary condition can overestimate the diffusivity for such one-dimensional diffusion because of the unrealistic collective movement of mobile ions.

The migrations in O4 column including the getting-out guidepaths are in good agreement with the nuclear density distribution of oxygen ions measured by the neutron powder diffraction [33]. In this nuclear density distribution, O<sub>int</sub>-1 sites are connected to regular O3 sites in addition to the linearly-connected descriptions in the O4 column along the *c* axis, while a different conclusions of “O4 migration by the vacancy mechanism along the *c* axis” and “O3 migration by the interstitial mechanism through the O<sub>int</sub>-1 site” were mentioned.

The getting-out mechanisms also have a crucial role in the long-range migration in the *ab* plane. The long-range migration pathway in the *ab* plane as shown in fig 4.2.2(b) is formed by the repetition of the getting-out and the equivalent reverse getting-in mechanism with the short-range conduction connecting these two processes in the metastable zone. The short conduction in the metastable zone is rate-determining pathway, whose potential barrier is 0.61 eV with reference to the most stable site

energy. This is almost the same value to 0.58 eV of the long-range migration along the  $c$  axis at the large- $N$  limit, which implies the nearly-isotropic oxygen-ion conduction along the  $c$  axis and in the  $ab$  plane.

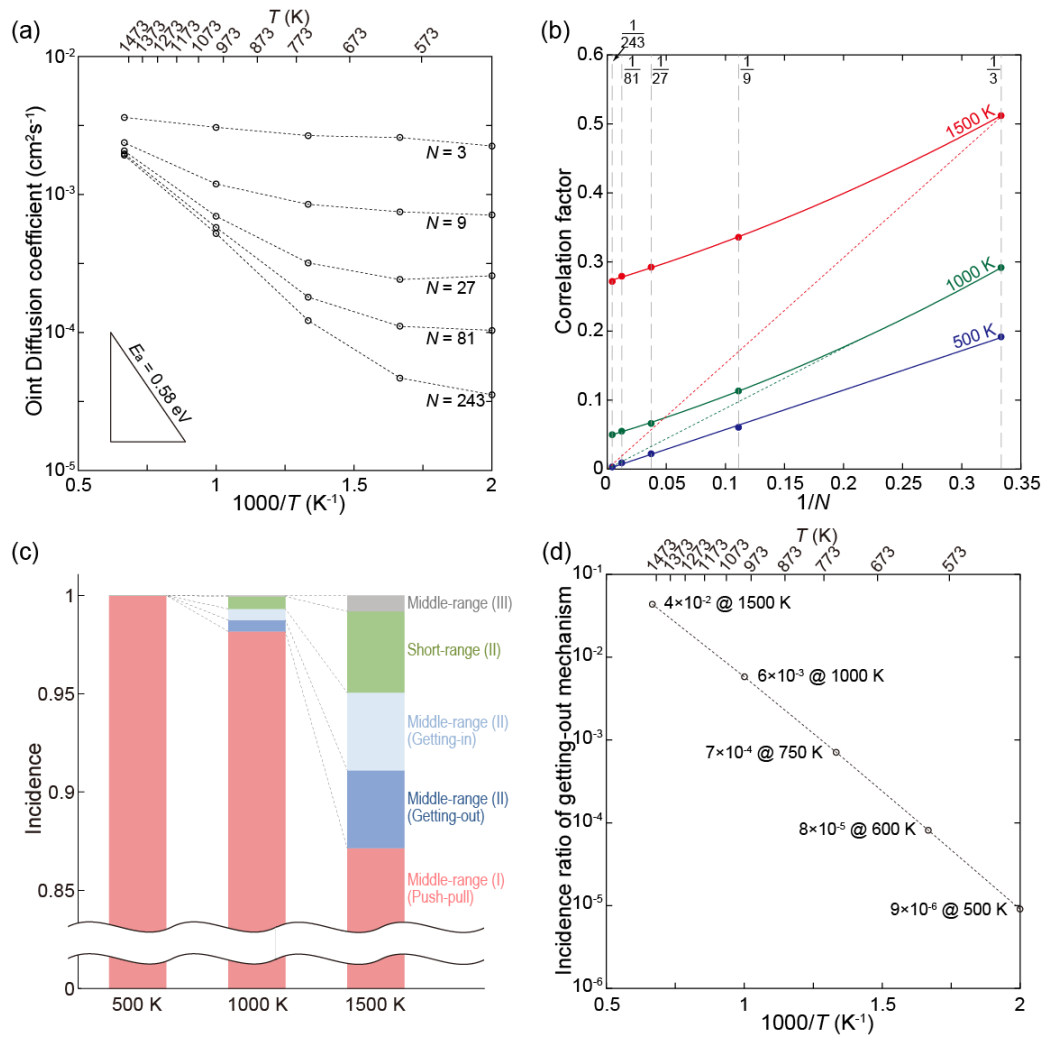


**Figure 4.2.3.** (a) The diffusion coefficients of the interstitial ions along the  $c$  axis calculated by the KMC simulations at the range of 500-1500 K against the inverse temperature  $1000/T$ . The  $1 \times 1 \times N$  unit cells of  $N = 3, 9, 27, 81$  and  $243$  were used in this KMC simulations with the periodic boundary condition. (b) The correlation factors of the interstitial-ion diffusion against the inverse supercell size  $N^{-1}$  at 500, 1000, and 1500 K. The hypothetical  $N^{-1}$  linear dependence of correlation factors were denoted by dotted lines. (c) The event rates of each migration process during the simulations at 500, 1000, and 1500 K. (d) The event ratio of the getting-out mechanism to the push-pull mechanism against  $1000/T$ .

### 4.2.3. Comparison with Previously Reported Mechanisms

The potential barriers of the long-range conduction along the  $c$  axis and in the  $ab$  plane are evaluated as comparable values of 0.58 eV and 0.61 eV, respectively, from the above simulations and discussions for the diffusion of interstitial ions in the lanthanum silicate. These potential barrier heights are consistent with the apparent activation energies of 0.6-0.7 eV measured experimentally in randomly-oriented crystal grains of  $\text{La}_{10}(\text{SiO}_4)_6\text{O}_3$ . On the other hand, the oxygen-ion conductivity in lanthanum silicate,  $\text{La}_{9.33+0.67x}(\text{SiO}_4)_6\text{O}_{2+x}$  ( $0.03 \leq x \leq 0.49$ ) which is highly-oriented along the  $c$  axis have been reported recently by Fukuda *et al.*, which indicates the large anisotropy of the oxygen-ion conduction due to the discrepancy of the apparent activation energy between 0.35 eV along the  $c$  axis and 0.71 eV in the  $ab$  plane [32,34]. Nakayama *et al.* are also reported the anisotropy of the oxygen ion conduction in the recent conductivity investigations using single crystal of  $\text{La}_{9.33}(\text{SiO}_4)_6\text{O}_2$  [35], which suggests the different pre-exponential factor of the conductivity,  $\sigma_0$  between along the  $c$  axis and in the  $ab$  plane is the main reason of the anisotropic conductivity in single crystal. The gradients of the oxygen-ion conductivity curves both along the  $c$  axis and in the  $ab$  plane corresponding to the apparent activation energies show comparable value of  $\sim 0.7$  eV. The potential barriers of the oxygen-ion conduction in the present study

are qualitatively consistent with the measured conductivities by the Nakayama *et al.* in light of the coincident potential barriers along the  $c$  axis and in the  $ab$  plane.

However, the present theoretical results cannot be compared simply to their experimental conclusions because each compositions  $x$  in  $\text{La}_{9.33+0.67x}(\text{SiO}_4)_6\text{O}_{2+x}$  is different. In fact, a number of La vacancies are involved in the experimental crystals ( $x < 0.5$ ) while the ideal crystal with noLa vacancies were used in the present theoretical study ( $x = 1$ ). Our previous analysis of conduction behaviors for interstitial ion in the  $\text{La}_{9.33}(\text{SiO}_4)_6\text{O}_2$  indicates that La vacancies drastically affect the potential energy surface (PES) of interstitial ions [10]. In addition, the potential barrier of the push-pull mechanism in the O4 column shows relatively higher with  $\sim 0.3$  eV in  $\text{La}_{9.33}(\text{SiO}_4)_6\text{O}_2$ , although that in the  $ab$  plane is lowered down to  $\sim 0.4$  eV. This means mean jump frequencies between the push-pull mechanism along the  $c$  axis and the getting-out mechanism in the  $ab$  plane is almost the same, which suggest the blocking effect in the O4 columns is rarely happened because the getting-out processes are occurred with frequency.

Moreover, compared to the oxygen conduction mechanisms in  $\text{La}_{10}(\text{GeO}_4)_6\text{O}_3$ , the migration pathways and mechanisms in  $\text{La}_{10}(\text{SiO}_4)_6\text{O}_3$  indicate large differences despite showing the same crystal structures. Especially, the migration paths of the extremely low potential barrier along the O4 column in  $\text{La}_{10}(\text{SiO}_4)_6\text{O}_3$  are not

existed in  $\text{La}_{10}(\text{GeO}_4)_6\text{O}_3$ , whose discrepancy is resulted from the discordance of the interstitial oxygen-ion sites between  $\text{La}_{10}(\text{SiO}_4)_6\text{O}_3$  and  $\text{La}_{10}(\text{GeO}_4)_6\text{O}_3$ . On the other hand, the long-range pathways in the *ab*-plane are performed by similar migration mechanisms via the O4 columns between both crystals, while the potential barrier of 0.61 eV in  $\text{La}_{10}(\text{SiO}_4)_6\text{O}_3$  is a little lower than 0.76 eV in  $\text{La}_{10}(\text{GeO}_4)_6\text{O}_3$ . This energy gap 0.15 eV is suggested that the stability of the O4 columns decreases by introduced interstitial oxygen ions at the O4 columns in  $\text{La}_{10}(\text{SiO}_4)_6\text{O}_3$  resulting in the potential barriers of getting out from/ into the O4 column processes to decrease.

Thus, La vacancies and compositions of  $\text{MO}_4$  (M = Si or Ge) tetrahedra in addition to the impurities and dopants in realistic systems make the interstitial oxygen ions migration mechanism more confounded. Conversely, it can make the oxygen ion conductivities of apatite-type lanthanum silicates drastically improved to the possible strategy for materials design that the interactions of blocking effect in the O4 column is controlled by the configurations and concentrations of La vacancies, dopants and  $\text{MO}_4$  unit compositions in the crystal.

## Chapter 5

### Effect of Lanthanum-ion Vacancies on Oxygen-ion Conduction

In this chapter, the similar theoretical analyses with those in chapter 3 and 4 were done to investigate the oxygen-ion conduction mechanism in  $\text{La}_{9.33}(\text{GeO}_4)_6\text{O}_2$  having La vacancies. An effect of La-ion vacancies on oxygen-ion conduction was discussed by comparing conduction mechanism in  $\text{La}_{9.33}(\text{GeO}_4)_6\text{O}_2$  with that in  $\text{La}_{10}(\text{GeO}_4)_6\text{O}_3$ .

#### 5.1 Interstitial Oxygen-ion Sites

Figure 5.2.1 shows the interstitial oxygen-ion sites with each local structure in  $\text{La}_{9.33}(\text{GeO}_4)_6\text{O}_2$ . There are energetically different four interstitial oxygen-ion sites, whose potential energies are 0.20 eV (O5-1), 0.26 eV (O5-2) and 0.33 eV (O5-3) with reference to the lowest potential energy site (O5-0). The representative positions of O5-0 to O5-3 are (0.48, 0.44, 0.18), (0.49, 0.54, 0.34), (0.52, 0.58, 0.50) and (0.44, 0.48, 0.32) in the fractional coordinate, respectively, whose crystallographically equivalent 6 sites exist per an interstitial site in  $1 \times 1 \times 3$  unitcells. As shown in figure 5.2.1(b), the energetically equivalent sites represented by the same color ball are located on the *ab*-planes. All interstitial oxygen-sites are located between two  $\text{GeO}_4$  tetrahedra, and as their local

structures in the figure 5.2.1(c),  $\text{Ge}_2\text{O}_9$  units are formed around the O5-0, O5-1 and O5-3 sites, although the  $\text{GeO}_5$  hexahedra structure is formed around the O5-2 site.

The interstitial oxygen-ion positions which are located between two  $\text{GeO}_4$  tetrahedra are similar with those in  $\text{La}_{10}(\text{GeO}_4)_6\text{O}_3$  (see the chapter 3.1). However, the interstitial sites in the  $\text{La}_{9.33}(\text{GeO}_4)_6\text{O}_2$  have several different site energies ( $\sim 0.33$  eV) along the  $c$ -axis. This discrepancy can be explained by taking the interactions between La vacancy ( $V_{\text{La}}$ ) and interstitial oxygen ion and the local structure around the interstitial sites into the consideration.

The positions of  $V_{\text{La}}$  and interstitial oxygen-ion sites with their distances are shown in figure 5.2.2 and table 5.2.1. The most stable interstitial site (O5-0) was located with the fractional coordinate of (0.48, 0.44, 0.18), which is slightly deviated from the center position, (0.5, 0.5, 0.17) reported in  $\text{La}_{10}(\text{GeO}_4)_6\text{O}_3$ . This shift of the interstitial site is considered to result from electrostatic repulsion between the interstitial oxygen-ion ( $\text{O}^{2-}$ ) and the  $V_{\text{La}}$  having the -3 charge. Therefore, it can be said that the smaller the distance between the interstitial and  $V_{\text{La}}$  sites is, the higher the site energy of the interstitial oxygen ion is. In fact, the O5-2 site which is the closest to the  $V_{\text{La}}$  site has the highest site energy of 0.33 eV. However, the farthest interstitial site of O5-2 from  $V_{\text{La}}$  site does not correspond to the lowest site energy, which means the site energy is not determined from the only single factor.

The interstitial oxygen ions in lanthanum germanates are stabilized to

form the  $\text{Ge}_2\text{O}_9$  units or  $\text{GeO}_5$  hexahedra as the local structures which covalently and ionically bonding to the Ge ions. The  $\text{Ge}_2\text{O}_9$  unit equally bonding two  $\text{GeO}_4$  tetrahedra is considered to be more stable local structure than the  $\text{GeO}_5$  hexahedron whose interstitial oxygen ion is shifted toward one  $\text{GeO}_4$  tetrahedron. Therefore, O5-2 site have comparatively higher site energy even though the distance from the  $V_{\text{La}}$  is the longest in four interstitial sites.

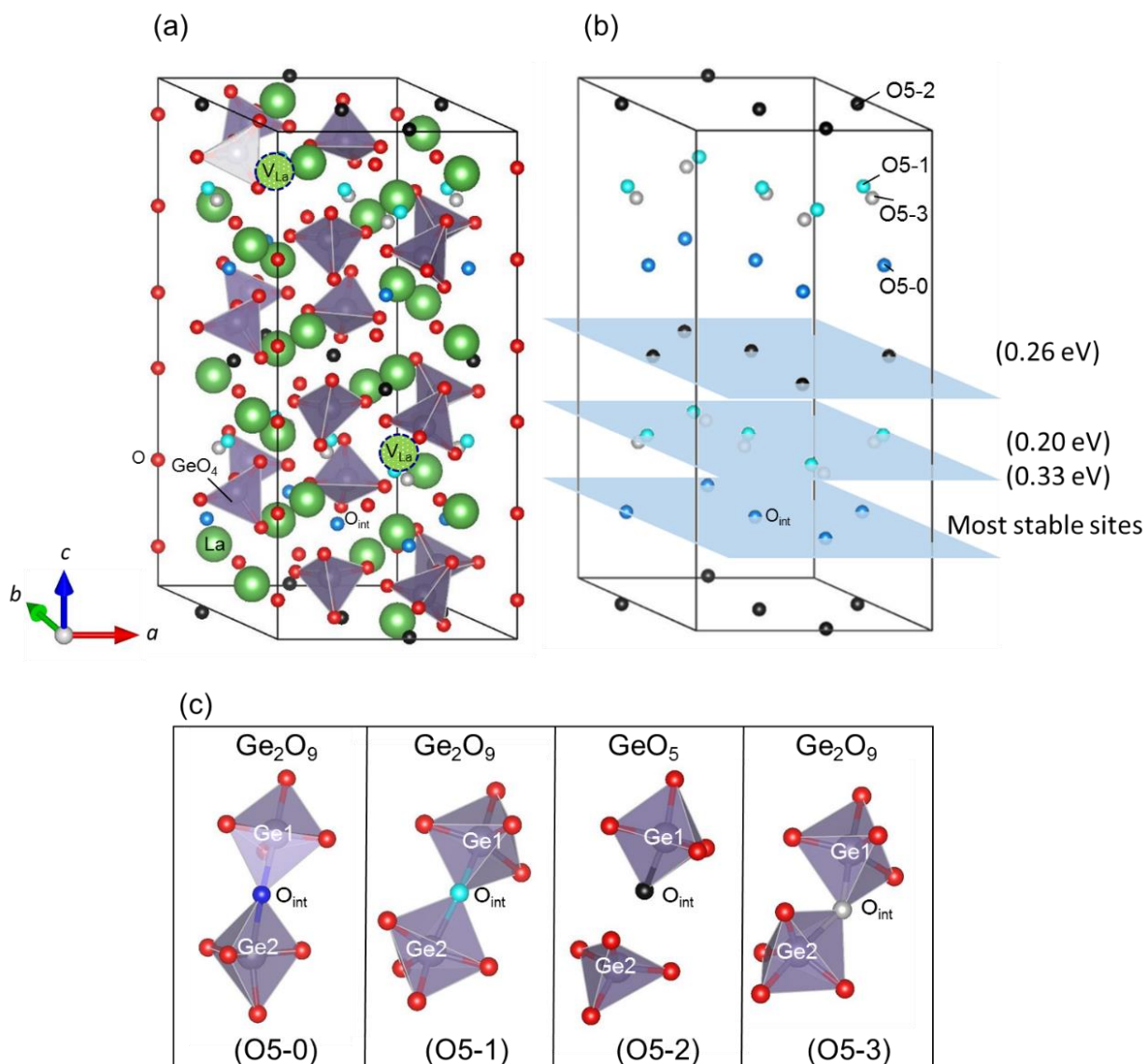


**Figure 5.2.1 (a) The stable sites of the interstitial oxygen ions in the crystal. (b) The equivalent interstitial sites of four stable sites (c) The local structures around each interstitial sites**

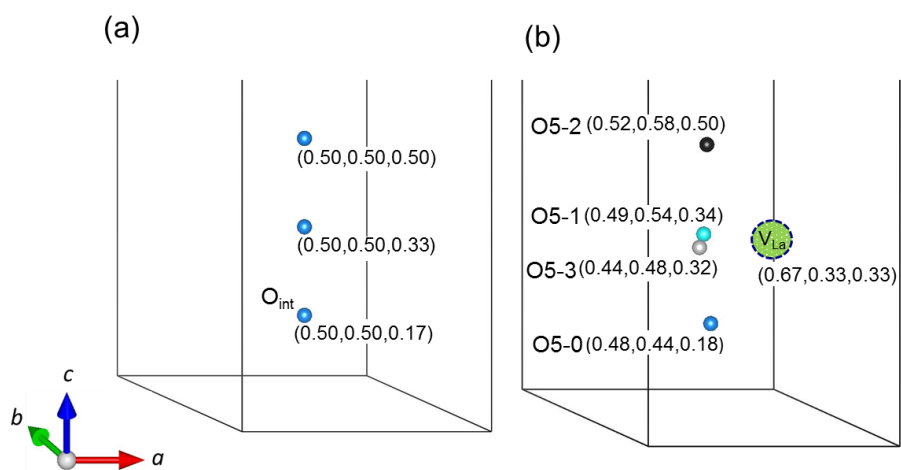


**Figure 5.2.2 The fractional coordinates for the stable interstitial sites in (a)  $\text{La}_{10}(\text{GeO}_4)_6\text{O}_3$  (b)  $\text{La}_{9.33}(\text{GeO}_4)_6\text{O}_2$**

**Table 5.2.1 Distances between  $V_{La}$  and interstitial sites**

$x = 0$	<b>O5-0</b>	<b>O5-1</b>	<b>O5-2</b>	<b>O5-3</b>
$V_{La} - O_{int}$ (Å)	4.21	3.32	5.02	3.24
$x = 1$	$O_{int}$ (0.5,0.5,0.17)	$O_{int}$ (0.5,0.5,0.33)	$O_{int}$ (0.5,0.5,0.5)	$O_{int}$ (0.5,0.5,0.33)
$La - O_{int}$ (Å)	4.54	2.91	4.70	2.91

## 5.2 Oxygen-ion conduction mechanisms in $\text{La}_{9.33}(\text{GeO}_4)_6\text{O}_2$

In this chapter, the conduction pathways connecting the obtained interstitial sites were calculated using the same methodology for  $\text{La}_{10}(\text{GeO}_4)_6\text{O}_3$  in chapter 4. The interstitial and interstitialcy conduction mechanisms and their energy profiles were considered for possible migration pathways both along the  $c$ -axis and in the  $ab$ -plane.

The interstitial migration processes along the  $c$ -axis were firstly considered. However, the potential barriers for all migration processes directly connecting between interstitial sites arranged along the  $c$ -axis indicated the high values in the range from 1.25 to 1.93 eV. On the other hand, the interstitial oxygen-ion can migrate with lower potential barriers by the cooperative interstitialcy mechanism. Figure 5.2.3 shows the conduction pathways by the interstitialcy mechanism along the  $c$ -axis with the lowest potential barrier. In this process, the interstitial oxygen ion at O5-0 site pushes the oxygen-ion at the regular site toward O5-1 site, and these cooperative elementary processes were conducted between O5-1 and O5-2 sites, and O5-2 and O5-0 sites, which become the long-range pathway by repeating three elementary processes. The potential energy of this conduction pathway is 0.92 eV, which is the dominant process along the  $c$ -axis. This dominant pathway and mechanism are almost the same with those in  $\text{La}_{10}(\text{GeO}_4)_6\text{O}_3$ , although the potential barrier of 0.92 eV is by 0.28 eV higher than 0.64 eV in  $\text{La}_{10}(\text{GeO}_4)_6\text{O}_3$ .

As for the oxygen-ion conduction in the  $ab$ -plane, migration

mechanisms between the neighboring interstitial sites were calculated. Interstitial and interstitialcy mechanisms were taken into consideration, and yet all their potential barriers indicated the significantly high, 1.3-6.1 eV. Next, the conduction mechanism via the O4 column which is reported as the dominant process in  $\text{La}_{10}(\text{GeO}_4)\text{O}_3$  was considered. Figure 5.2.4 shows three elementary processes between the interstitial sites via the O4 column whose potential barriers are lower than 1 eV. Potential barriers of the migrations from O5-0 to (a) O5-2, (b) O5-1 and (c) O5-0 are 0.73 eV, 0.94 eV and 0.99 eV, respectively. The long-range conduction pathways in the *ab*-plane, however, are not formed only by the combinations and repetitions of these three elementary migrations. The other elementary processes via the O4 column are over 1 eV in all, which are necessary to form the long-range conduction pathways in the *ab*-plane. The long-range pathway having the lowest potential barrier, 1.26 eV, by repeating the elementary process via the O4 column is shown in figure 5.2.5. In order to circumvent the high potential paths, the conduction pathway along the *c*-axis is combined as the bypass in the *ab*-plane pathways as shown in figure 5.2.6. The potential barrier decreases to 0.92 eV, which shows the same dominant process of the long-range pathway along the *c*-axis.

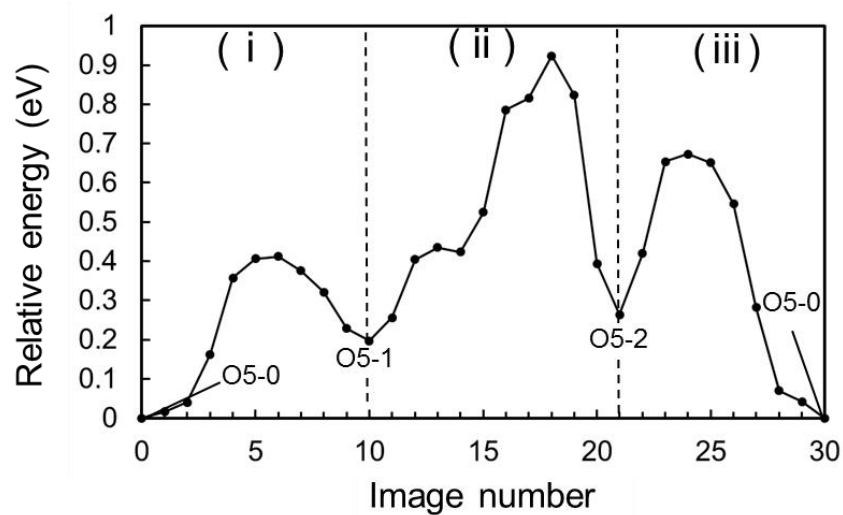
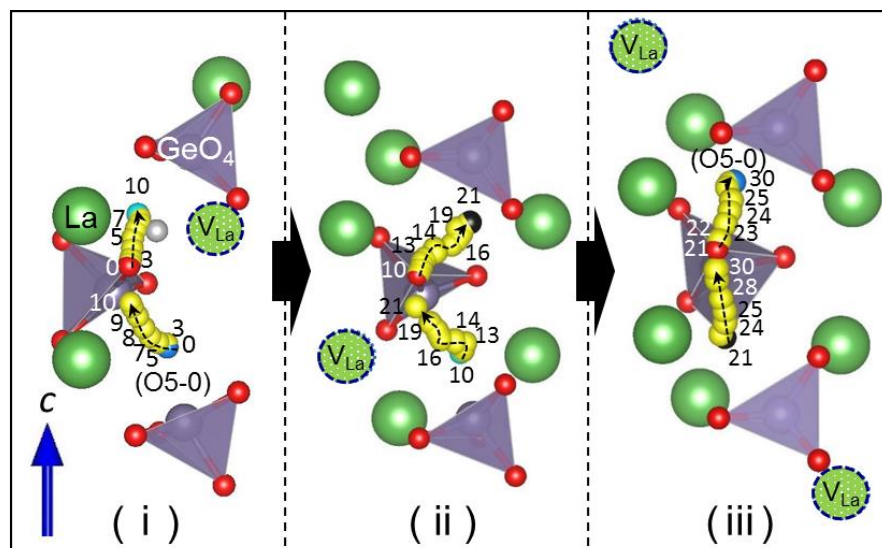


**Figure 5.2.3 The interstitialcy mechanisms and their energy profiles along the *c*-axis**

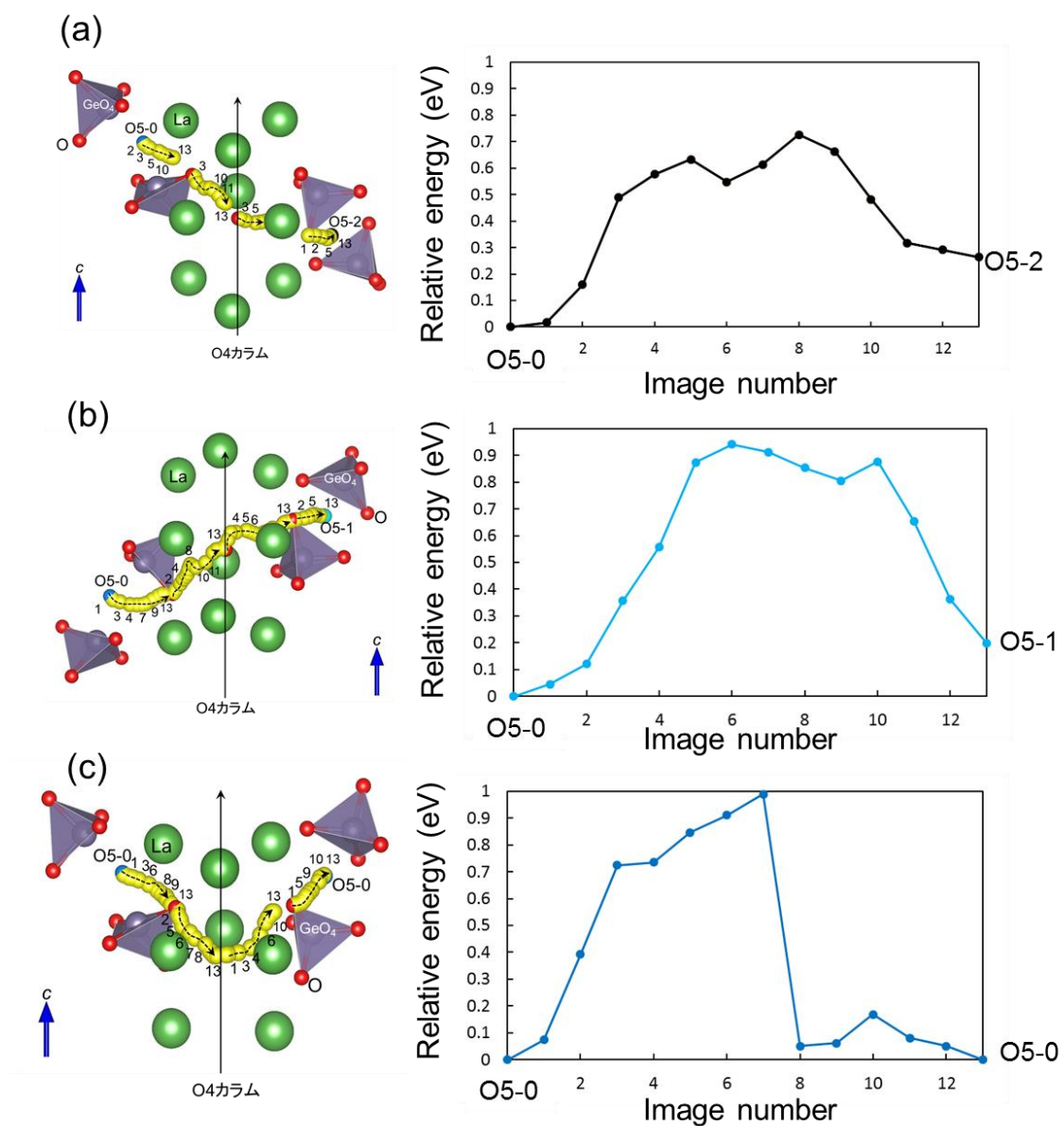


**Figure 5.2.4** The elementary processes of the cooperative conduction via the O4 column from (a) O5-0 to O5-2, (b) O5-0 to O5-1 and (c) O5-0 to O5-0

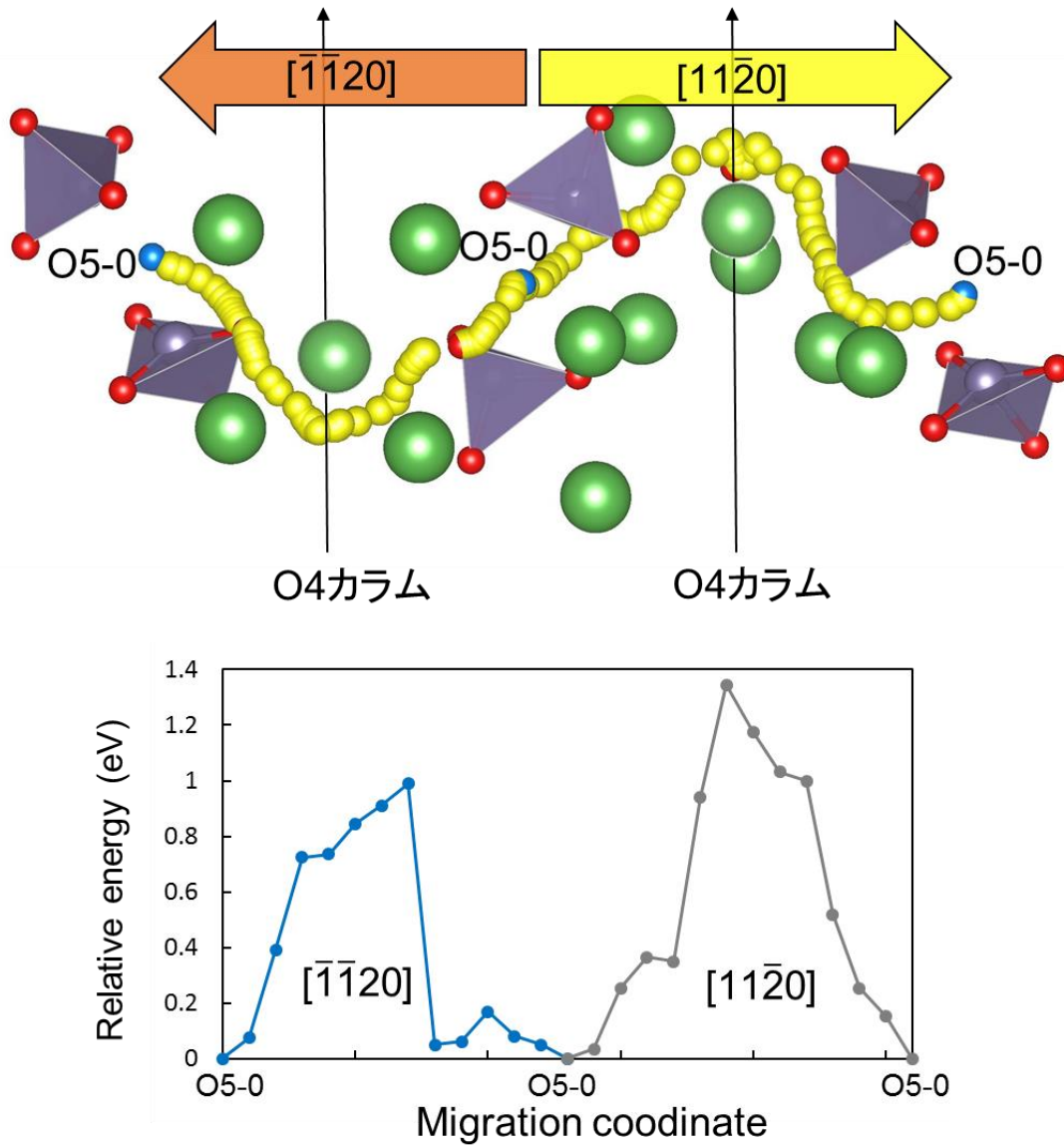


**Figure 5.2.5** The long-range pathway and energy profile of the conduction via the O4 column.

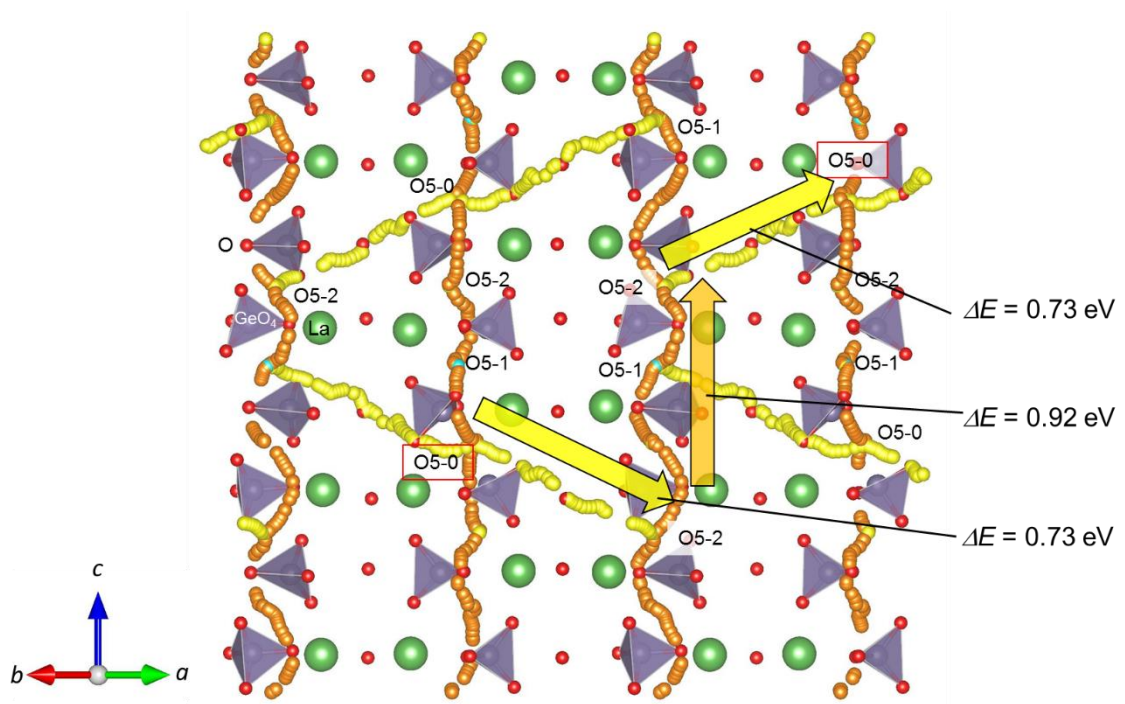


**Figure 5.2.6** The dominant conduction pathways in the  $\text{La}_{9.33}(\text{GeO}_4)_6\text{O}_2$ .

### 5.3 Comparison with Reported Theoretical mechanisms

Comparing the above conduction mechanisms and these energy profiles in  $\text{La}_{9.33}(\text{GeO}_4)_6\text{O}_2$  to those in  $\text{La}_{10}(\text{GeO}_4)_6\text{O}_3$ , the dominant conduction pathways and the mechanism (i.e. cooperative interstitialcy mechanism along the  $c$  axis) are in good agreement between two compositions. On the other hand, the potential barriers of the conduction pathways both along the  $c$  axis and in the  $ab$  plane in  $\text{La}_{9.33}(\text{GeO}_4)_6\text{O}_2$  totally tend to be higher than those in  $\text{La}_{10}(\text{GeO}_4)_6\text{O}_3$ . Especially, the potential barriers of the dominant long-range conduction pathways in  $\text{La}_{9.33}(\text{GeO}_4)_6\text{O}_2$  and  $\text{La}_{10}(\text{GeO}_4)_6\text{O}_3$  are 0.92 eV and 0.64 eV, respectively as shown in figure 5.2.7. This energy gap of 0.28 eV is almost correspond to the site energy of O5-2 site, 0.26 eV, which suggests that the increase of potential barriers in  $\text{La}_{9.33}(\text{GeO}_4)_6\text{O}_2$  results from the difference of the site energies of the interstitial oxygen ion between  $\text{La}_{9.33}(\text{GeO}_4)_6\text{O}_2$  and  $\text{La}_{10}(\text{GeO}_4)_6\text{O}_3$ .

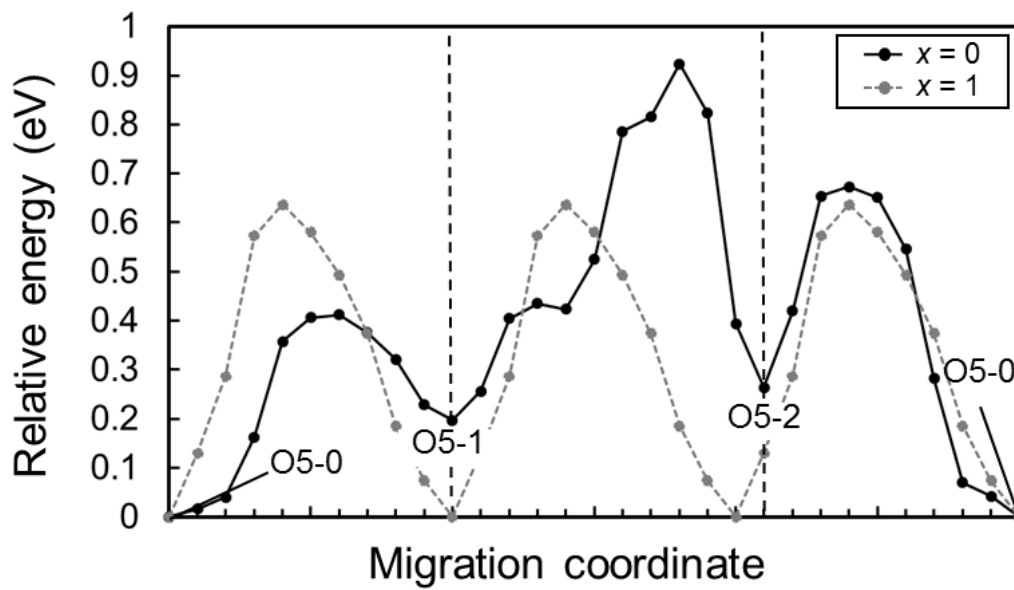


**Figure 5.2.7** The energy profiles of dominant conduction pathway in  $\text{La}_{9.33}(\text{GeO}_4)_6\text{O}_2$  (solid line) and  $\text{La}_{10}(\text{GeO}_4)_6\text{O}_3$  (broken line).

## Chapter 6

### General Conclusion

First-principles calculations were performed to investigate the oxygen-ion conduction mechanisms in the lanthanum silicate and germanate in the present study. At first, the stable sites of interstitial oxygen ion which are closely related to oxygen-ion migrating behaviors were determined in the two systems,  $\text{La}_{10}(\text{GeO}_4)_6\text{O}_3$  and  $\text{La}_{10}(\text{SiO}_4)_6\text{O}_3$ , which showed the reasonable agreements with the previous-reported interstitial sites. In addition, the difference of the interstitial sites between at the interspace of two  $\text{GeO}_4$  tetrahedra in  $\text{La}_{10}(\text{GeO}_4)_6\text{O}_3$  and at the periphery of the O4 column in  $\text{La}_{10}(\text{SiO}_4)_6\text{O}_3$  was suggested to be caused by the different atomic coordinations for Ge and Si ions in their oxygen phases.

The potential barriers of the possible oxygen-ion conduction paths between the determined interstitial sites  $\text{La}_{10}(\text{GeO}_4)_6\text{O}_3$  and  $\text{La}_{10}(\text{SiO}_4)_6\text{O}_3$  were evaluated by the NEB methods. As a result, it was found that the potential barriers of the long-range conduction pathways along the  $c$  axis vs. in the  $ab$  plane are almost the same with 0.64 eV vs. 0.76 eV in  $\text{La}_{10}(\text{GeO}_4)_6\text{O}_3$  and 0.58 eV vs. 0.61 eV in  $\text{La}_{10}(\text{SiO}_4)_6\text{O}_3$ , which were in good agreement with the experimental activation energy. In the conduction mechanism, the cooperative conduction processes with several oxygen-ions at interstitial and regular sites were found to be dominant

rather than the simple interstitial mechanism. However, the detail conduction processes were different due to the difference in the stable interstitial sites between  $\text{La}_{10}(\text{GeO}_4)_6\text{O}_3$  and  $\text{La}_{10}(\text{SiO}_4)_6\text{O}_3$ . The individual summaries are shown in the followings.

In  $\text{La}_{10}(\text{GeO}_4)_6\text{O}_3$ , the most stable interstitial sites were determined at the center between the two neighboring  $\text{GeO}_4$  tetrahedra. The potential barriers of long-range conduction pathways along the  $c$ -axis and in the  $ab$ -plane evaluated by the NEB method were 0.64 eV and 0.76 eV, respectively, which indicate the nearly isotropic oxygen-ion conduction. The estimated oxygen-ion conductivity by the KMC simulation was in good agreement with the reported conductivity curve in the temperature region corresponding to the hexagonal high-temperature phase.

In  $\text{La}_{10}(\text{SiO}_4)_6\text{O}_3$ , on the other hand, the most stable and the two metastable interstitial sites were found at the periphery of the O4 column and between two neighboring  $\text{SiO}_4$  tetrahedra, respectively. The oxygen-ion conduction pathway in the O4 column has been believed the fast long-range conduction pathway, but it was revealed that interstitial oxygen ions cannot migrate over a long range through the one-dimensional column in the case of realistic-scale crystals due to the blocking effects between neighboring mobile interstitial ions. Instead, the migration process getting out the O4 columns was here proposed to play a key role for the long-range conduction not only along the  $c$  axis but also in the  $ab$  plane. This process can relax the blocking effect in the column along the  $c$  axis and is also a part of the long-range conduction pathway in

the *ab* plane. The calculated potential barrier is 0.58 eV, which almost determines the apparent activation energies of both conductivities along the *c* axis and in the *ab* plane.

In order to estimate the effects of the La vacancy to the oxygen-ion conduction, the interstitial sites and conduction mechanisms in  $\text{La}_{9.33}(\text{GeO}_4)_6\text{O}_2$  having La vacancies were calculated by the same methods of  $\text{La}_{10}(\text{GeO}_4)_6\text{O}_3$ . The interstitial sites were located between two neighboring two  $\text{GeO}_4$  tetrahedra, which mostly coincide with the interstitial sites in  $\text{La}_{10}(\text{GeO}_4)_6\text{O}_3$  although the several different site energies were found because the crystallite symmetry in  $\text{La}_{9.33}(\text{GeO}_4)_6\text{O}_2$  was decayed by introducing La vacancies. The dominant conduction pathway along the *c* axis was in good agreement with that in  $\text{La}_{10}(\text{GeO}_4)_6\text{O}_3$ , but its potential barrier of 0.92 eV was higher than the potential height of 0.68 eV in  $\text{La}_{10}(\text{GeO}_4)_6\text{O}_3$ . Since this energy difference of 0.28 eV corresponds to the site energy through during migrations, it was suggested that the lowering of the crystallite symmetry by La vacancy causes the rise of potential barriers for the oxygen-ion conduction, which corresponds to the increasing tendency of activation energy when the La vacancies introduce in lanthanum germanate.

## References

- [1] S. Nakayama, H. Aono, Y. Sadaoka, *Chem. Lett.*, 1995, **6**, 43.
- [2] S. Nakayama, M. Sakamoto, *J. European Ceram. Soc.*, 1998, **18**, 1413.
- [3] H. Arikawa, H. Nishiguchi, T. Ishihara, Y. Takita, *Solid State Ion.*, 2000, **136**, 31.
- [4] H. Yoshioka, *J. Am. Ceram. Soc.*, 2007, **90**, 3099.
- [5] L. Leon-Reina, E. R. Losilla, M. Martinez-Lara, S. Bruque, M. A. G. Aranda, *J. Mater. Chem.*, 2004, **14**, 1142.
- [6] L. Leon-Reina, J. M. Porras-Vazquez, E. R. Losilla, M. A. G. Aranda, *Solid State Ion.*, 2006, **177**, 1307.
- [7] M. S. Islam, J. R. Tolchard, P. R. Slater, *Chem. Commun.*, 2003, **13**, 1486.
- [8] A. Jones, P. R. Slater, M. S. Islam, *Chem. Mat.*, 2008, **20**, 5055.
- [9] E. Bechade, O. Masson, T. Iwata, I. Julien, K. Fukuda, P. Thomas, E. Champion, *Chem. Mat.*, 2009, **21**, 2508.
- [10] K. Matsunaga, K. Toyoura, *J. Mater. Chem.*, 2012, **22**, 7265.
- [11] S. S. Pramana, W. T. Klooster, T. J. White, *Acta Crystallogr. Sect. B-Struct. Sci.*, 2007, **63**, 597.
- [12] E. Kendrick, M. S. Islam, P. R. Slater, *Chem. Commun.*, 2008, **6**, 715.
- [13] P. M. Panchmatia, A. Orera, G. J. Rees, M. E. Smith, J. V. Hanna, P. R. Slater, M. S. Islam, *Angew. Chem.-Int. Edit.*, 2011, **50**, 9328.

- [14] J. D. Gale, *J. Chem. Soc.-Faraday Trans.*, 1997, **93**, 629.
- [15] B. G. Dick, A. W. Overhauser, *Physical Review*, 1958, **112**, 90.
- [16] P. E. Blochl, *Phys. Rev. B*, 1994, **50**, 17953.
- [17] G. Kresse, J. Hafner, *Phys. Rev. B*, 1993, **47**, 558.
- [18] G. Kresse, J. Hafner, *Phys. Rev. B*, 1993, **48**, 13115.
- [19] G. Kresse, J. Hafner, *Phys. Rev. B*, 1994, **49**, 14251.
- [20] G. Kresse, J. Furthmuller, *Comput. Mater. Sci.*, 1996, **6**, 15.
- [21] G. Kresse, J. Furthmuller, *Phys. Rev. B*, 1996, **54**, 11169.
- [22] J. P. Perdew, K. Burke, M. Ernzerhof, *Phys. Rev. Lett.*, 1996, **77**, 3865.
- [23] G. Henkelman, B. P. Uberuaga, H. Jonsson, *J. Chem. Phys.*, 2000, **113**, 9901.
- [24] K. A. Fichthorn, W. H. Weinberg, *J. Chem. Phys.*, 1991, **95**, 1090.
- [25] A. Van der Ven, G. Ceder, M. Asta, P. D. Tepesch, *Phys. Rev. B*, 2001, **64**, 184307.
- [26] A. Orera, M. L. Sanjuan, E. Kendrick, V. M. Orera, P. R. Slater, *J. Mater. Chem.*, 2010, **20**, 2170.
- [27] Y. Q. Zhang, Z. X. Su, A. K. Azad, W. Z. Zhou, J. T. S. Irvine, *Adv. Energy Mater.*, 2012, **2**, 316.
- [28] E. Kendrick, M. S. Islam, P. R. Slater, *J. Mater. Chem.*, 2007, **17**, 3104.
- [29] E. J. Abram, C. A. Kirk, D. C. Sinclair, A. R. West, *Solid State Ion.*, 2005, **176**, 1941.
- [30] S. S. Pramana, T. Baikie, E. Kendrick, M. K. Schreyer, P. R. Slater, T.

- J. White, *Solid State Ion.*, 2010, **181**, 1189.
- [31] S. Nakayama, M. Sakamoto, M. Higuchi, K. Kodaira, M. Sato, S. Kakita, T. Suzuki, and K. Itoh, *J. European. Ceram. Soc.*, 1999, **19**, 507
- [32] K. Fukuda, T. Asaka, M. Okino, A. Berghout, E. Bechade, O. Masson, I. Julien, and P. Thomas, *Solid State Ionics.*, 2012, **217**, 40
- [33] R. Ali, M. Yashima, Y. Matsushita, H. Yoshioka, K. Ohoyama, and F. Izumi, *Chem. Mater.*, 2008, **20**, 5203
- [34] K. Fukuda, T. Asaka, M. Oyabu, D. Urushihara, A. Berghout, E. Bechade, O. Masson, I. Julien and P. Thomas, *Chem. Mater.*, 2012, **24**, 4623
- [35] S. Nakayama, A. Ikesue, Y. Higuchi, M. Sugawara, and M. Sakamoto, *J. Eur. Ceram. Soc.*, 2013, **33**, 207
- [36] S. Guillot, S. Beaudet-Savignat, S. Lambert, RN. Vannier, P. Rouse and F. Porcher, *J. Solid State Chem.*, 2009, **12**, 3358

## **Acknowledgements**

The author would like to express my sincere gratitude to his advisor, Professor Katsuyuki Matsunaga for offering him the a lot of precious opportunity to finish the doctor course in Department of Materials Science and Engineering, Nagoya University, and also for countless valuable discussions and advices during the last three years. The author is also grateful to Professor Takahisa Yamamoto and Yasutoshi Iriyama at Nagoya University, Dr. Akihide Kuwabara at Japan Fine Ceramics Center and Associate Professor Kazuaki Toyoura for reading my thesis.

Special thanks go to Associate Professor Atsutomo Nakamura for his valuable discussions and helpful advices to his study and preparation of his presentation during the last two years.

The author is grateful to Doctor for Tatsuya Yokoi for his technical assistances and continuous advices, which have been significant supports in completing this thesis.

The author is thankful to Mrs. Ayumi Nagao for her help with accounting work and daily affairs. The author would like to thank all the members in Professor Matsunaga's group for their continuous encouragement and useful discussions.

Finally, the author would like to sincerely thank his family for their continuous support and understanding and encouragement.

## Publication list

### Original Papers

1. K. Imaizumi, K. Toyoura, A. Nakamura, K. Matsunaga, “Stable sites and diffusion pathways of interstitial oxide ions in lanthanum germanate”, *Solid State Ionics*, 262, 512-516, 2014.
2. K. Imaizumi, K. Toyoura, A. Nakamura, K. Matsunaga, “Strong correlation in 1D oxygen-ion conduction of apatite-type lanthanum silicate”, *Journal of Physics: Condensed Matter*, 27 , 365601-365608, 2015.
3. K. Imaizumi, K. Toyoura, K. Matsunaga, “Conduction behavior of interstitial oxide-ion in apatite-type oxide-ion conductors”, *AMTC Letters*, 5 , 110-111, 2016.
4. K. Imaizumi, K. Toyoura, A. Nakamura, K. Matsunaga, “Cooperative oxide-ion conduction in apatite-type lanthanum germanate - A first principles study”, *Journal of the Ceramic Society of Japan*, 125, 105-111, 2017.

## **Presentations at International Conferences**

1. K. Imaizumi, K. Toyoura, A. Nakamura, K. Matsunaga, “Cooperative Conduction Mechanisms of Interstitial Oxide Ions in Apatite-Type Lanthanum Germanate and Silicate”, The 2013 MRS Fall Meeting & Exhibit, (Boston, USA), 1-6 Dec. 2013, Poster presentation
2. K. Imaizumi, K. Toyoura, A. Nakamura, K. Matsunaga, “First-Principles Analysis of Oxide-Ion Conductions in Apatite-Type Lanthanum Silicate and Germanate”, 2nd International Symposium on Frontiers in Material Science (FMS2015), (Tokyo, Japan), 19-21 Nov. 2015, Oral presentation
3. K. Imaizumi, K. Toyoura, K. Matsunaga, “Conduction behavior of interstitial oxide-ion in apatite-type oxide-ion conductors”, The 5th International Symposium on Advanced Microscopy and Theoretical Calculations, (Nagoya, Japan), 11-13 May 2016, Poster presentation